Gene Expression during Aortic Arch Development and Remodeling in Chick Embryos

-A Time Lapsed Network Analysis

by

Cansu Karakaya

A Thesis Submitted to the

Graduate School of Sciences and Engineering

in Partial Fulfillment of the Requirements for

the Degree of

Master of Science

in

Biomedical Sciences and Engineering

KOÇ UNIVERSITY

January 23, 2018

To my family,

ABSTRACT

Embryonic aortic arches (AA) are bilaterally paired, transitional vessels that are subjected to large-scale vascular morphogenesis and remodeling. Failures in AA patterning based on hemodynamic and growth-related adaptations cause a spectrum of congenital heart disease (CHD) anatomies. It is critical to identify regulatory mechanisms and cross-talk between the genetic elements of these vessels to understand the etiology of CHD and incorporate this information to refine predictive computational models. In our previous work, we reconstructed the three-dimensional (3D) time-lapsed growth data of chick AA in terms of vessel diameter and wall shear stress (WSS) values. The current study aims to screen expression profiles of fundamental biological pathways in the AA at early embryonic Hamburger & Hamilton Stages (HH) of 18, 21 and 24 in the chick embryo, and correlate these data with our previous vascular growth and mechanical loading results. RT-qPCR was performed for angiogenesis, cardiovascular development, and structural and apoptosis-related genes for the left and right lateral arches. Correlation and novel peak expression analysis were conducted in order to compare the behavior and activation period of the associated genes. Available protein networks were integrated with our time-resolved data to investigate the interactions between molecules and highlight major hierarchies to be used in future computational predictions. Based on these analyses, two types of expression patterns, correlated to changes in WSS and diameter, were detected. It was observed that the WSS has a major effect in the regulation of genetic activity, which may contribute to the early left/right patterning of aortic arches. Effect of WSS was seen directly on angiogenesis-related genes other than TGFβ2 as well as extracellular matrix, cytoskeleton and apoptosis-related genes. Our time-resolved network demonstrated that genes correlated with the WSS coordinate the activity of critical growth factors such as VEGF, FGF8 and TGFβ2. Moreover, differences in the gene expression of left and right AA might be an indicator of later asymmetric morphogenesis of the AA. These findings may further our understanding of the complex processes of cardiac morphogenesis and errors that result in CHD.

ÖZETÇE

Embriyonik aortik arklar (AA), büyük ölçekli vasküler morfogeneze ve yeniden şekillenmeye maruz kalan, bilateral olan çifte yerleşimli damarlardır. Hemodinamik ve büyümeyle ilişkili AA adaptasyonundaki başarısızlık, bir dizi konjenital kalp hastalığı (KKH) anatomisine neden olur. KKH etiyolojisini anlamak için bu damarların genetik öğeleri arasındaki düzenleyici mekanizmaları ve çapraz etkileşimi tanımlamak ve prediktif hesaplama modellerini arıtmak için bu bilgiyi birleştirmek kritik önem taşır. Önceki çalışmamızda, tavuk embriyonik AA'nın damar çapı ve duvar kesme gerilimi (WSS) değerleri açısından üç boyutlu hızlandırılmış büyüme verilerini yeniden yapılandırdık. Mevcut çalışma, tavuk embriyosunda Hamburger & Hamilton Evreleri (HH) 18, 21 ve 24'te AA'daki temel biyolojik yolların ekspresyon profillerini taramak ve bu verileri önceki vasküler büyüme ve mekanik yükleme sonuçlarımız ile ilişkilendirmeyi amaçlamaktadır. RT-qPCR, anjiogenezis, kardiyovasküler gelişme ve sol ve sağ lateral arkuslar için yapısal ve apoptoz ile ilgili genler için gerçekleştirildi. İlişkili genlerin davranış ve aktivasyon periyotlarını karşılaştırmak için korelasyon ve yeni zirve ekspresyon analizi yapıldı. Kullanılabilir protein ağları, moleküller arasındaki etkileşimleri araştırmak ve gelecekteki hesaplama tahminlerinde kullanılabilecek büyük hiyerarşileri vurgulamak için zamana göre çözümlenmiş verilerle entegre edildi. Bu analizlere dayanarak, WSS ve çaptaki değişikliklerle bağlantılı iki tip ekspresyon trendi tespit edildi. Aortik arkların erken dönemde sol / sağ olarak biçimlendirilmesine katkı sağlayabilecek genetik aktivitenin düzenlenmesinde WSS'nin önemli bir etkisi olduğu gözlemlendi. WSS'nin etkisi, doğrudan TGFβ2 dışındaki anjiyojenezle ilişkili genlerin yanı sıra hücre dışı matris, sitoskeleton ve apoptoz ile ilişkili genler üzerinde görüldü. Zamana göre çözümlenmiş ağımız, WSS ile ilişkili genlerin, VEGF, FGF8 ve TGFβ2 gibi kritik büyüme faktörlerinin aktivitesini koordine ettiğini gösterdi. Dahası, sol ve sağ AA'nın gen ekspresyonundaki farklılıklar, AA'nın daha sonraki asimetrik morfogenezinin bir göstergesi olabilir. Bu bulgular, kardiyak morfogenezin karmaşık süreçleri ve KKH'na neden olan sorunlar hakkındaki anlayışımızı daha da ilerletebilir.

ACKNOWLEDGEMENTS

I would like to acknowledge my advisor, Dr. Kerem Pekkan for his constant support and assistance over the course of my graduate study. I am very pleased that I had an opportunity to study in an interdisciplinary laboratory environment thanks to him.

I would like to thank all of my lab mates and colleagues who were extremely friendly and supportive in all situations. It was great pleasure for me working with all of you!

I would like to thank European Research Council (ERC) - Vascular Growth Project for the scholarship provided.

Also, I would like to thank Graduate School of Science and Engineering, Koç University for their patient administrative and logical support.

TABLE OF CONTENTS

List of Figures

List of Tables

Nomenclature

AA	Embryonic aortic arches
ACTA2	alpha smooth muscle actin
ANGPT1	Angiopoietin 1
ANGPT2	Angiopoietin 2
BMP2	Bone morphogenetic protein 2
CASP3	Caspase 3
CDH5	Cadherin 5 (vascular endothelial cadherin)
CHD	Congenital heart disease
COL1	Collagen I
COL3	Collagen III
COL4	Collagen IV
EC	Endothelial cells
ECM	Extracellular matrix
ED	Embryonic day
ELN	Tropoelastin
ET1	Endothelin 1
FBN1	Fibrillin 1
FGF8	Fibroblast Growth Factor 8
FN1	Fibronectin 1
HAND2	Heart and neural crest derivatives expressed 2
HH	Hamburger & Hamilton
HHEX	Hematopoietically expressed homeobox protein
HOXA3	Homeobox protein A3
ICAM1	Intercellular cell adhesion molecule 1
LSS	Steady laminar shear stress

MMP	Matrix metalloproteinase
MMP2	Matrix metalloproteinase 2
NOS3	Nitric oxide synthase 2
OFT	Outflow tract
OSS	Oscillatory shear stress
PITX2	Paired-like homeodomain transcription factor 2
PSS	Pulsatile shear stress
RT-qPCR	Real time reverse transcriptase quantitative polymerase chain reaction
RVA	Right vitelline artery
SHH	Sonic hedgehog
SMAD2	SMAD family member 2
SMC	Smooth muscle cells
TBX1	T-box transcription factor 1
TGFβ1	Transforming growth factor β1
TGFβ2	Transforming growth factor β2
TGFβ3	Transforming growth factor β3
TIMP	Tissue inhibitor of matrix metalloproteinase
TIMP2	Tissue inhibitor of metalloproteinase 2
TIMP3	Tissue inhibitor of metalloproteinase 3
TSS	Turbulent shear stress
VCAM1	Vascular cell adhesion molecule 1
VCL	Vinculin
VEGF	Vascular endothelial growth factor
WSS	Wall shear stress

Chapter 1. Introduction

1.1 Embryonic Vascular Development

Heart is the first functional organ to materialize in the body, however it cannot start beating until the vasculature forms in parallel and they integrate. There are two important steps for vascular formation and development; Vasculogenesis is the *de novo* formation of blood vessels from mesoderm and Angiogenesis is the later sprouting and remodeling of the vessels.

In vasculogenesis, cells migrating from primitive streak becomes hemangioblasts which further differentiate into hematoblasts to form blood cells and angioblasts that are responsible in forming the blood vessels [1]. Further, angioblasts proliferate and differentiate into endothelial cells (EC) which line the blood vessels [2]. EC coalescence and lumenize to form primary capillary plexus. Vascular endothelial growth factor (VEGF) signalling is essential in this process [2]. Primary capillary plexus is later remodelled by angiogenesis.

Angiogenesis is initiated with an increase in vascular permeability by VEGF. VE-cadherin (CDH5) is one of the mediators of this mechanism. Angiopoietin 1 (ANGPT1) act as a balance for vascular permeability since excess permeability might cause vascular leakage which is not desired for a functionally intact lumen. Afterwards, EC start to migrate by detaching their cellular contacts. Angiopoietin 2 (ANGPT2) and matrix metalloproteinases (MMPs) enable the detachment and degrading of extracellular matrix (ECM), respectively [3]. EC responding to signals and sprouting are called tip cells, and they are the leading cells to find the paths. Tip cells expand filopodia to sense the signals and moves to the right directions with their lamellipodia. The remaining cells, stalk cells, are able to proliferate which allow them to form the structural body of the vessels [1]. Finally, vascular mural cells which inhibit the proliferation and migration of EC are recruited to form the vessel wall, and produce ECM to stabilize the vessels [3].

Angiopoietins have significant roles in vascular remodeling and stabilization [2]. In this process, ANGPT1 promotes stabilization of the vessel by triggering the interaction between mural cells and EC [3], and ANGPT2 acts as its agonist. ANGPT2 is expressed in local sites of remodeling to promote destabilization. In the presence of VEGF, this destabilization results in vessel remodeling, but when VEGF is absent, vessel regresses because of apoptotic EC [2].

1.2 Embryonic Aortic Arch Morphogenesis

At the embryonic stage, blood is transported from the heart to the dorsal aorta through the bilaterally paired aortic arch (AA) system. AA are arisen from aortic sac and become the vasculature of pharyngeal arches. They appear in cranio-caudal fashion as pairs at early development, and numbered I-VI; later, undergo extensive remodeling which is critical to give rise to proper asymmetric vascular network.

In humans, pair of AA I form portions of maxillary artery while pair of AA II form portions of stapedial artery. Left and right AA III form left and right carotid arteries, respectively. Left AA IV persists and constitutes the aortic arch segment while right AA IV forms right subclavian artery. Proximal parts of left and right AA VI form left and right proximal portions of pulmonary arteries, respectively. Distal portion of left AA VI becomes ductus arteriosus– another transient arterial vessel left for the preterm circulatory adjustments while right AA VI involutes. AA V occasionally appear in development and does not contribute to any mature vessel [4, 5].

Proper remodeling of AA in embryonic development is critical since it affects significant circulatory mechanisms. When both right and left AA IV persist, they cause double aortic arch formation. Abnormal involution of left AA IV results right-sided aortic arch with aberrant left subclavian artery. If the entire right dorsal aorta involutes, left aortic arch with aberrant right subclavian artery is seen. Infants with aortic arch anomalies generally require surgical treatment for correction [4].

1.3 Hemodynamic Forces and Wall Shear Stress

Large blood vessels, such as the great vessels that emerge from the heart, are composed of three layers: tunica intima, tunica media and tunica adventitia. Tunica intima is composed of a layer of EC which line the lumen. Basement membrane is located adjacent to tunica intima and provides support for EC. Tunica media is composed of smooth muscle cells (SMC) and ECM, particularly elastin and collagens, and it regulates vascular tone by changing the diameter of the vessel. Tunica adventitia is the outer layer of the vessel and composed of connective tissue, fibroblasts, loose ECM and small vessels to supply the vascular wall [6]. Blood flow implements mechanical forces directly to the tunica intima, and EC lining the vessel transduce these mechanosignals to other layers in order to adapt accordingly.

Mechanosensation is carried out by primary cilia, glycocalyx which is a jelly structure surrounding the apical membrane of EC, ion channels and adhesion molecules. They take the mechanosignals and convert them to biological responses by changing the organization of cytoskeleton [7].

Shear stress, specifically wall shear stress (WSS) is one of the effective mechanical forces that is exerted directly to EC. It is driven by the blood flow and it is parallel to the cross section of the vessel. WSS is directly proportional to flow, thus different flow regimes affect the response of EC. Laminar flow in straight vessels is generally associated with EC quiescence, SMC relaxation and vasodilation. On the other hand, disturbed flow in curvatures makes the EC to give an inflammatory response [7].

The role of hemodynamic forces on development and remodeling of vasculature, particularly in AA, has been shown with different experimental models. In mouse embryos, the side of the aortic arch is determined by blood flow. Spiral structure of the outflow tract (OFT) rotates 90^{o} during cardiac looping, thus changing the symmetrical blood flow through the pair of AA VI. Left AA VI starts to take increased flow compared to right AA VI which decreases in diameter and eventually regresses. This asymmetric flow distribution results in the formation of left-sided aortic arch because the side of the aortic arch depends on the side that AA VI regresses. Left and right AA VI of the mouse embryos in which OFT rotation is genetically prevented take equal flow, so right AA VI persists, and the side of aortic arch randomly determined [8]. In chick embryos, venous clip model in which right vitelline vein is ligated shows the effect of WSS on cardiac development and AA remodeling. Alteration in intracardiac flow pattern results in several cardiovascular abnormalities such as ventricular septal defects, and semilunar valve anomalies. AA malformations included the persistence of left AA IV leading to double aortic arch, deformations in AA IV leading to interruption of aorta, and decrease in the diameter of right AA III and VI [9].

1.4 Chick Embryo as a Model Organism to Study Cardiovascular Development

Chick embryos having 4-chambered mature hearts, have been used to study cardiovascular development for years due to their resemblance to human development [10, 11] . Moreover, they are suitable to easy manipulation and imaging.

In humans, cardiac development starts at 3rd week of gestation and is completed at 8th week of gestation whereas in chick embryos, it starts at Hamburger & Hamilton (HH) [12] Stage 8, embryonic day (ED) 2, and is completed at HH39, ED 13. Heart develops as a tube at first, and loops into an S shape with the clockwise rotation of cranial portion and counter-clockwise rotation of caudal portion. After remodeling, it becomes single-chambered, and finally it is divided into four chambers with the development of endocardial cushions and septa [10]. Chick embryos undergo AA selection similar to humans with few differences. In humans, left AA IV persists and become the part of left-sided mature aortic arch while in chick, right AA IV persists and makes the aortic arch right-sided. Moreover, in chick embryos, both laterals of AA VI persist until after hatching; however, in humans, right AA VI regress earlier [11].

1.5 Gene Expression Profiling Methods

DNA includes the genetic code which needs to be converted into functional products to regulate vital activities by a process called gene expression. Different genes are expressed in different frequencies at different times, and they can be examined by profiling their expression with several ways some of which are introduced below.

One of the old methods is northern blot technique which is used to detect RNA. This method is accomplished with electrophoresis for the separation of RNA, transferring separated RNA to a membrane, hybridization with a labelled probe and running on a gel. Although northern blot gave its place to more sensitive RNA detection methods, it is still used to identify the transcript size.

Real time reverse transcriptase quantitative polymerase chain reaction (RT-qPCR) is a rapid and sensitive way to detect gene expression. In this method, isolated RNA samples are transcribed into cDNA which are specifically amplified with the presence of fluorescent dyes. During the amplification, the dyes in gene copies are detected by the machine which allows the monitoring of the cycle real-time. It provides threshold cycle (C_t) numbers based on the concentration of the products, and expression profiles can be determined with absolute or relative quantification with using C_t.

DNA microarrays are used to detect the expressions of thousands of genes at once. Each spot in microarray includes oligomers specific to desired genes, and fluorescently-labelled cDNA samples hybridize with the oligomers. Hybridization levels with the detection of fluorescent quantifies the expression. Although its coverage in terms of gene number is high, the utilization of the arrays is hard and commercially available arrays have high costs.

In our experiments, we used RT-qPCR method to determine gene expression levels due to its high sensitivity and relatively small number of genes to be analyzed [13].

The aim of this thesis is to examine the expression levels of genes involving to different biological pathways which enhance the development and asymmetric remodeling of AA in chick embryos at HH18, HH21 and HH24. Moreover, we hypothesize to find correlative interactions between gene expression and hemodynamics and growth data obtained in our previous studies for the same developmental stages. More comprehensive information including time, hemodynamic changes and gene expression can be determined by this means and used to understand the complex process of AA development whose normal morphogenesis mechanism is critically important to reveal the pathogenesis of CHD.

Chapter 2. Gene Expression and Network Analysis during AA Morphogenesis

2.1 Introduction

Congenital heart disease (CHD) is the most common type of cardiac disorder that occurs approximately 8 of every 1000 live births [14]. In order to survive, severely cyanotic patients require immediate open-heart surgeries as soon as they are born and further interventions throughout their lifetime [15]. CHDs develop due to either new genetic mutations or epigenetic insults that alter cardiac morphogenesis *in utero.* Previous data have shown that embryonic cardiovascular systems dynamically regulate structure and function over very short time periods, and biomechanical loading conditions within the heart and aortic arches affect vascular morphology and the future genetic expression.

Embryonic aortic arches (AA) are central in the prognosis of major CHD anatomies. AA vessels are transient and undergo regression and remodeling to form the great arteries of adult circulation [4]. At the embryonic stage, blood is transported from the heart to the dorsal aorta through the bilaterally paired AA system. Six paired AA appear symmetrically and consecutively, then they selectively regress and remodel during development resulting an *asymmetric* vasculature during a relatively short time period. The cause of asymmetry in AA has been associated with Pitx2-mediated pathways [16], but more comprehensive investigations are needed.

In our previous descriptive studies, we measured the WSS and diameter of each AA in chick embryos for HH18 and 24 [17], and later HH21 [18]. At HH18 (ED 3), AA II, III and IV and at HH24 (ED 4), AA III, IV and VI were observed in all chick embryos. However, HH21 (ED 3.5) was a unique stage in which four different vascular configurations of AA could be seen. 2AA configuration included AA III and IV; 4AA configuration included AA II, III, IV, VI; 3AA-cranial configuration was similar to HH 18 and included AA II, III, IV; 3AA-caudal configuration was similar to HH24 and included AA III, IV, VI. In all cases, the configuration of AA system was symmetrical, so the left and right AA were observed together, but the WSS and diameter measures were significantly different. This asymmetric mechanical loading might therefore initiate the transition from symmetric to asymmetric system, which might influence the mechanosensitive gene expression levels, further augmenting the asymmetric development (Figure 2.1).

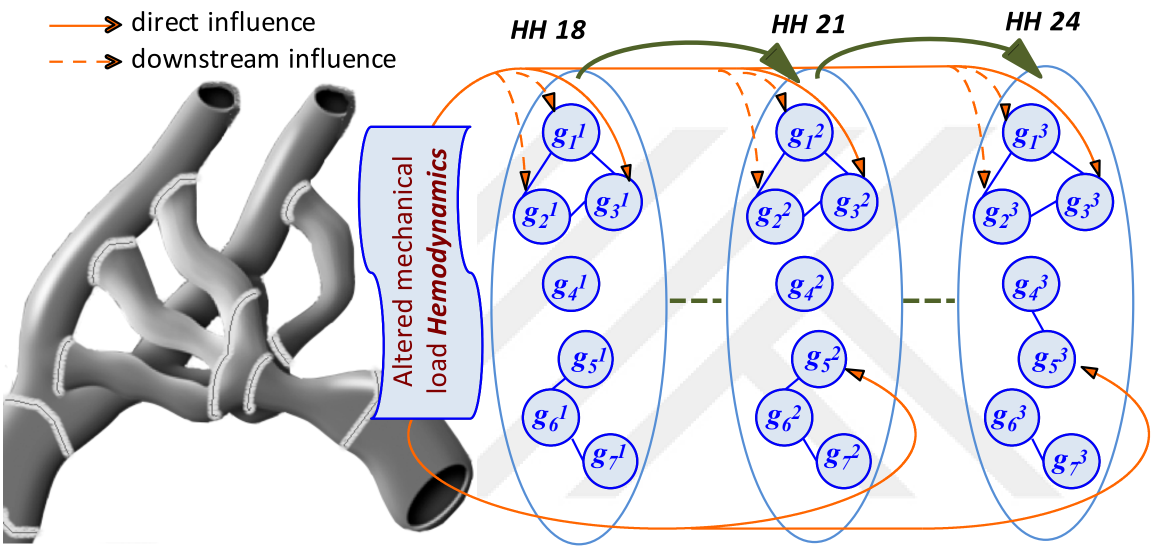

Figure 2.1 Interactions of major molecular pathways and individual genes (gi) with the mechanical loading during three embryonic time-points are illustrated. Schematic showing the predicted effects of altered mechanical loading on different biological pathways at stages HH18, HH21 and HH24.

Prior to further investigating this complex vascular apparatus, we studied the interactions among vascular growth, hemodynamics and gene expression in different developmental stages of chick embryo for the right vitelline artery (RVA) [19]. In this simpler arterial vessel, it was observed that the expression trends of angiogenesis- and apoptosis-related genes varied significantly despite the steady growth rates. WSS has a direct influence on *VEGF* expression, but *MMP2* and *CASP3* expressions were not affected by hemodynamic changes. In the same study, mechanosensitive genes *KLF2* and *NOS3* were expressed proportionally to WSS whereas *ET1* expression responded WSS with a significant time lag. Moreover, TGFβ and BMP signaling pathway gene *TGFβ3* had an expression trend proportional to pulsatile pressure. The relations and different patterns in gene expression of RVA with time encouraged us to investigate and compare the gene expression patterns in the AA system.

There are a small number of studies on gene expression trends within the AA in relation to asymmetric development. Mechanosensitive gene expression was investigated in the cardiovascular system of chick embryos. As a general trend, *KLF2* and *NOS3* expression were seen at high WSS areas while *ET1* was inversely related with WSS later in development. In AA, *KLF2* expression decreased, *ET1* expression increased and *NOS3* expression did not change between HH16-HH30 [20]. In another study, it was shown that unilateral ablation of *Pitx2* expression damages asymmetric vascular development [8]. Moreover, *Pitx2* expression changes the morphology of the outflow tract which result in the altered blood flow, and eventually changes in the expression of vascular endothelial and platelet-derived growth factor receptors.

In this study, we investigated the expression levels of genes related to angiogenesis, cardiovascular development and remodeling, ECM, cytoskeleton and apoptosis in AA of chick embryos at HH18, HH21 and HH24 to understand the correlation of gene expression with growth and hemodynamic changes and asymmetric development of AA system in later stages. Furthermore, a novel peak expression analysis of WSS-correlated genes allowed us to acquire integrated time-resolved information on the genetic pathways controlling AA development and morphogenesis, first time in literature.

2.2 Methods

Chick embryonic aortic arch (AA) collection

Fertilized White Leghorn chicken eggs (*Gallus gallus domesticus* L.) were incubated in an incubator (Kuhl Corp., New Jersey, USA) at constant humidity (67%) and temperature (37.5°C) (Figure 2.2 (A)). A small window was opened on the egg shell and tissue segment including all AA were collected at embryonic stages HH18, HH21 and HH24 using microsurgical tools [21]. Left-sided and right-sided aortic arch vessels were dissected out separately while removing the excess tissue around the vessels (Figure 2.2 (B)). Following extraction, left and right AA tissues were separately transferred to cold Krebs solution, then to RNAlater (Sigma Aldrich) for further analysis.

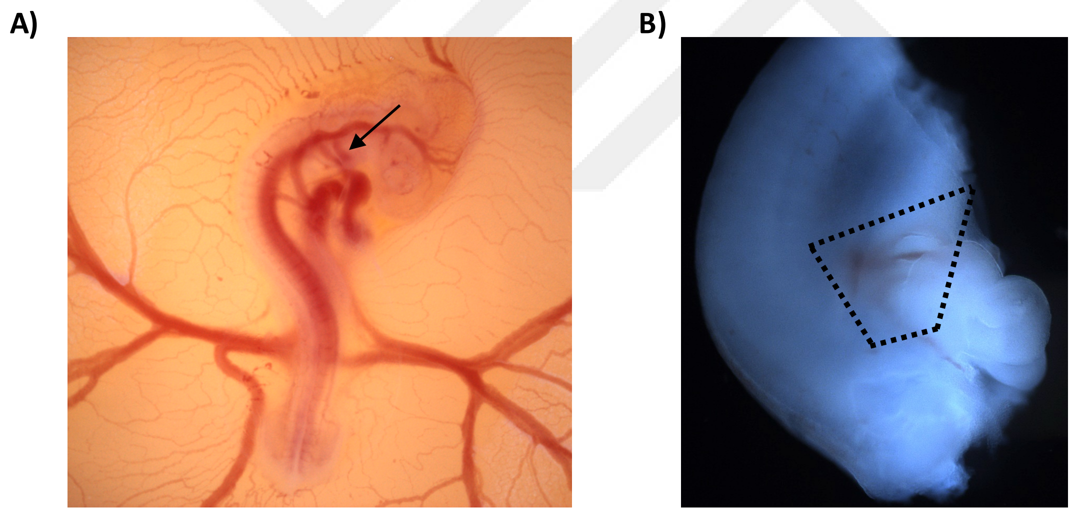

Figure 2.2 (A) Lateral view of the chick embryo at stage HH18. Arrow shows the AA vessels. **(B)** Dissected AA apparatus of chick embryos. Enclosed area shows the boundaries of right-sided AA used for analyses.

RT-qPCR analysis

Total RNA of pooled chick embryonic left and right AA (n = 4-7 embryos) was extracted using GeneJET RNA purification kit (Thermo Scientific) (Protocol A1). The purity and concentration of the RNA samples were quantified with NanoDrop 2000c spectrophotometer (Thermo Scientific). cDNA was then transcribed with Maxima First Strand cDNA Synthesis Kit (Thermo Scientific) (Protocol A2). Quantitative reverse transcription PCR (RT-qPCR) was performed using Luminaris Color HiGreen qPCR Master Mix (Thermo Scientific) (Protocol A3) to measure the expression levels for 20 genes in different biological pathways including angiogenesis (*ANGPT1, ANGPT2, TGFβ2, TGFβ3, CDH5, MMP2, TIMP3, VEGF*), cardiovascular development and remodeling (*NOS3, HHEX, TBX1, FGF8, ET1, HOXA3, HAND2, SHH*), ECM (*FN1, FBN1, ELN, COL1, COL3, COL4*), cytoskeleton (*ACTA2, VCL*) and apoptosis (*CASP3*). Forward and reverse primer sequences were designed with Beacon Designer Software (Table 2.1). Thermal conditions for the reaction were: initial denaturation at 95°C for 10 min followed by a three-step cycle of denaturation at 95°C for 15 s, annealing at 60°C for 30 s and extension at 72°C for 30 s, repeated 40 times. Only *ANGPT1* and *ELN* had unique annealing temperatures of 53°C and 62°C, respectively. *GAPDH* was chosen as control gene to normalize the relative expression levels of the genes using the $2^{-\Delta\Delta C_T}$ method [22]. Moreover, fold changes were determined based on HH18 left AA expressions for all genes.

Table 2.1: Forward and reverse primer sequences for the selected genes. Primer sequences were designed with Beacon Designer Software.

Gene Name	Forward(F) / Reverse(R)	Primer Sequence
ANGPT1	F	ATGGAGGAGGATGGACAGTT
	R	CATTTCCCAGCCAGTGTTCA
ANGPT2	F	AGGAGGGTGGTGGTTTGAT
	R	AGTCGTGGCTTTGAGAGAGT
ACTA2	F	GACTGAAGCACCACTGAATCC
	R	GAAGCATACAGGGACAGAACAG

CASP3	F	CAGATGCAAGATCTTTCCCTGG
	R	CCGGTATCTCGGTGGAAGTTC
CDH5	F	GAGCGGTCTCAGGAGGAAT
	R	GAGCACGGACACATCATAGC
COL1A2	F	CAAGAGGTCTCCCAGGTCAA
	R	TCCAATGTTGCCAGGTTCAC
COL3A1	F	ACAGGGAATGCCAGGAGAA
	R	AGGACCAGGAGGACCAATG
COL4A1	F	CCAAAGGACAGCAAGGAGTAAC
	R	GGAGGACCATAAGGACCAACT
ELN	F	TCAAGAGATGGCAAGGCAGG
	R	AAAAAGCCTCCTCCTGGGAC
ET1	F	CGAGGAGTGCGTGTATTTCTG
	R	CAGCAAGCATCTCTGGCATT
FN1	F	GCAGATCAGACCTCTTGCAC
	R	GTACCCAATAATGGTGGAGGC
FBN1	F	GAAGCAGAGGATGAGCAAGAG
	R	TGAGGGCAGGAAGCAGTT
FGF8	F	AGACCGACACCTTTGGGA
	R	CCTTGCCTTTGCCGTTACT
GAPDH	F	GATTCTACACACGGACACTTCA
	R	CTGAGGGAGCTGAGATGATAAC
HAND2	F	CCAGCTACATCGCCTACCT
	R	CCTTCTTCCTCTTCTCCTCCTT
HHEX	F	CTACACGCACGCACTGATC
	R	TGGTCTGCTCGTTGGAGAA
HOXA3	F	CTCTTCAAGGCAACGGTTATGG
	R	TTGGCAGAGGGAGGATGAG
MMP2	F	AGGTCGCAATGATGGCAAG
	R	GGCAGCAACCAAGAAGAGAC
NOS3	F	TGGTACATGAGCAGCGAGAT
	R	TCCAGAGGGACGAAGTCTTAC
SHH	F	GTCATCGAGGAGCACAGTTG
	R	AGGAGCCGTGAGTACCAAT
TBX1	F	GCTGTGGGACGAGTTCAAC
	R	GGTCCATGCCGAATATCTTCAC
TIMP3	F	CATCGTTATCATCTGGGCTGTG
	R	TCGCTTGGTGTCCTGAGT
TGFβ2	F	CAACTTGGTGAAGGCTGAGT
	R	GTAACGCTGTCCTGGTGATG
TGFβ3	F	TACCTCAGTGGCAGGAATGT
	R	GTATGCCAAGGGCAGTGTATG
VEGFA	F	CTTTCTGCTCACTTGGATCCAC
	R	GTCTCAATTGTCCTGCAGAAGC
VCL	F	CGACATCATTGCTGCTGCTA
	R	GTGACTTCATCCGATGCCTTAG

Average WSS and diameter calculation and trends

Data for the cardiac averaged WSS and vessel midpoint diameters were extracted for left and right AA from our previously published studies [17, 18]. Average WSS for HH18 and HH24 were calculated by taking the sum of WSS multiplied with its corresponding lumen surface area, and then dividing this sum to the total aortic manifold surface area. For WSS calculations of HH21, the observed probabilities of AA configurations were also taken into consideration [18]. Significant diameter changes were also calculated from our previous diameter measurements using optical coherence tomography [17, 18]. Total significant increase and/or decrease in individual arch diameters between HH18 and HH21 were treated as the changes at HH18 and between HH21 and HH24 were treated as the changes at HH24. Significant changes at HH21 were calculated by taking the average of changes at HH18 and HH24. At the end of these calculations, two trends, WSS-trend and growth-trend, were determined. WSS-trend was the change in average WSS with an increase through HH21 following a decrease through HH24. Although significant diameter change seems to decrease, the tissue size around the vessels increases based on our observations, meaning an increase in growth. Therefore, we determined the continuous increase in growth through HH24 as growth-trend. Furthermore, gene expression patterns were classified based on their similarity to WSS or growth-trends. Considering the gene expression temporal cascade (Figure 2.1), the WSS-trend is upstream whereas the growth-trend is downstream.

Correlation and Peak Expression Time

Gene expression values of left and right AA for each stage were plotted against averaged WSS values or significant diameter changes and classified according to the trend type the corresponding expressions followed (either the WSS-trend or the growth-trend). Coefficient of correlation (R) was assessed. A value of 0.8 was used as a cut-off for correlation with R.

Average of R values for left and right AA were calculated to assess the overall correlation of a gene expression. For genes following the WSS-trend, slopes were calculated from two gene expression points, and a polynomial curve was fitted using QtiPlot [23]. The time corresponding to the peak points of the fitted expression curve relative to the embryonic timeline were determined as the "peak expression time" values. Deviations more than 2.4 hours from HH21 time point were considered as early or late peak expression (Figure 2.3). WSS-trend genes were sorted first according to their correlation strength and the time of their peak expressions analysis was included only for the statistically significant correlations.

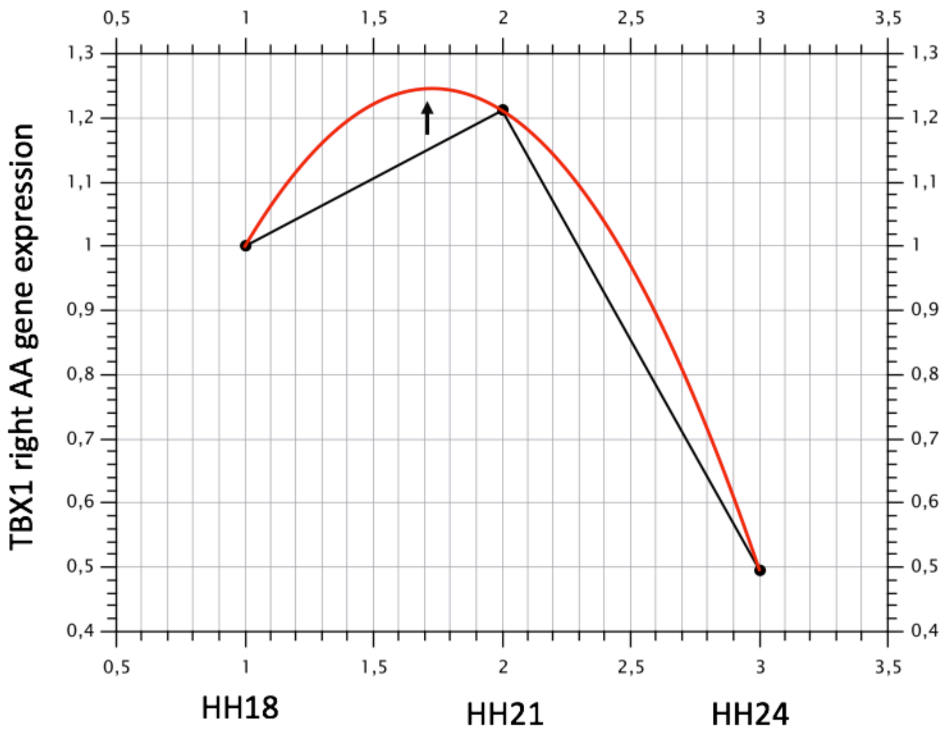

Figure 2.3 Determination of the peak expression time points. A second order polynomial curve (shown in red color) was fitted to the gene expression level measurement points at HH18, HH21 and HH24 for the genes following the WSS-trend with high correlation. Peak points of the curves (arrow) were determined as the corresponding peak expression time values. Peak points which deviated 2.4 hours from HH21were considered as early or late peak expression time.

Network Construction

Identifying the peak expression time allowed the ordering of molecular pathway maps as a function of the embryonic time. Gene/protein network interactions were determined using Search Tool for the Retrieval of Interacting Genes/Proteins (STRING) Database [24]. When some of the possible interactions (e.g. *NOS3* and *TBX1*) were not available for *Gallus gallus domesticus*, the organism was selected as *Homo sapiens*. Default parameters of the database were used to obtain the final network structure. All the active interaction sources were selected, and the minimum required interaction score was adjusted as 0.4. Moreover, molecular action mode was selected to see the molecular interactions between genes and proteins (Protocol A4).

Nodes were aligned in embryonic time according to their correlation level and peak expression time value. First, WSS-correlated and growth-correlated genes were grouped. The groups were aligned from left to right as WSS-correlated genes, WSS and growth-correlated genes (transition) and growth-correlated genes, respectively. Afterwards, within WSS-correlated genes, nodes were lined up based on their peak expression times. In addition, the nodes were arranged from top to bottom in descending order of correlation. Genes having R values below 0.8 were colored as brown and their alignment in the network is not considered to be statistically meaningful. Blue-colored nodes represent the highly-correlated genes and red-colored nodes represent the genes whose activities can be predicted.

Statistical Analysis

IBM SPSS Statistics v23 was used to perform statistical analysis. After determining the normal distribution and the homogeneity of the data, one-way analysis of variance (ANOVA) and post-hoc Tukey HSD were performed to assess the significance of gene expression and average WSS data. Statistical significance level was adjusted to $p<0.05$. All data was presented as mean ± standard deviation.

2.3 Results

WSS and Diameter

According to our calculations, averaged-WSS increased from HH18 to HH24, peaking for both left and right AA at HH21 (Figure 2.4). WSS changes between HH18 and HH21 ($p=0.001$ for left, $p=0.002$ for right), and also between HH21 and HH24 ($p=0.012$ for left, $p=0.005$ for right) were statistically significant while there was not a significant change on different laterals within stages. When changes in the individual diameters of AA were analyzed, it was seen that diameters of AA IV and AA VI significantly increased, and AA II significantly decreased between HH18 and HH21 for both left and right AA. AA VI diameter significantly increased for both laterals while AA IV diameter significantly increased for only right AA between HH21 and HH24 (Figure 2.5). These changes were summarized in significant diameter trend charts (Figure 2.6).

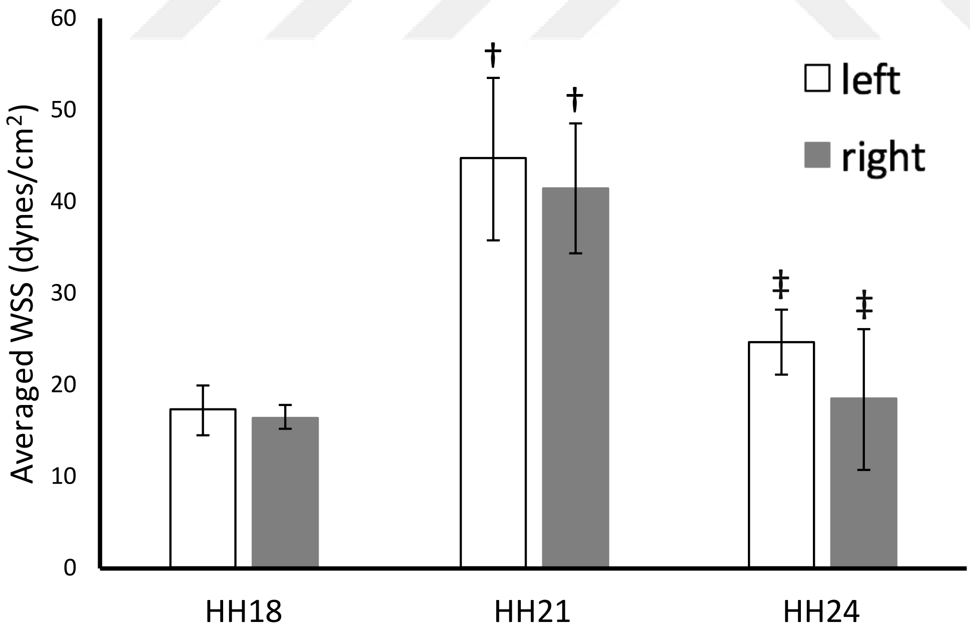

Figure 2.4 Averaged WSS of left and right AA for HH18, HH21 and HH24 with a peak at HH21. Following symbols indicate the statistical significant difference ($p<0.05$): † for difference in same side between HH18 and HH21; ‡ for difference in same side between HH21 and HH24.

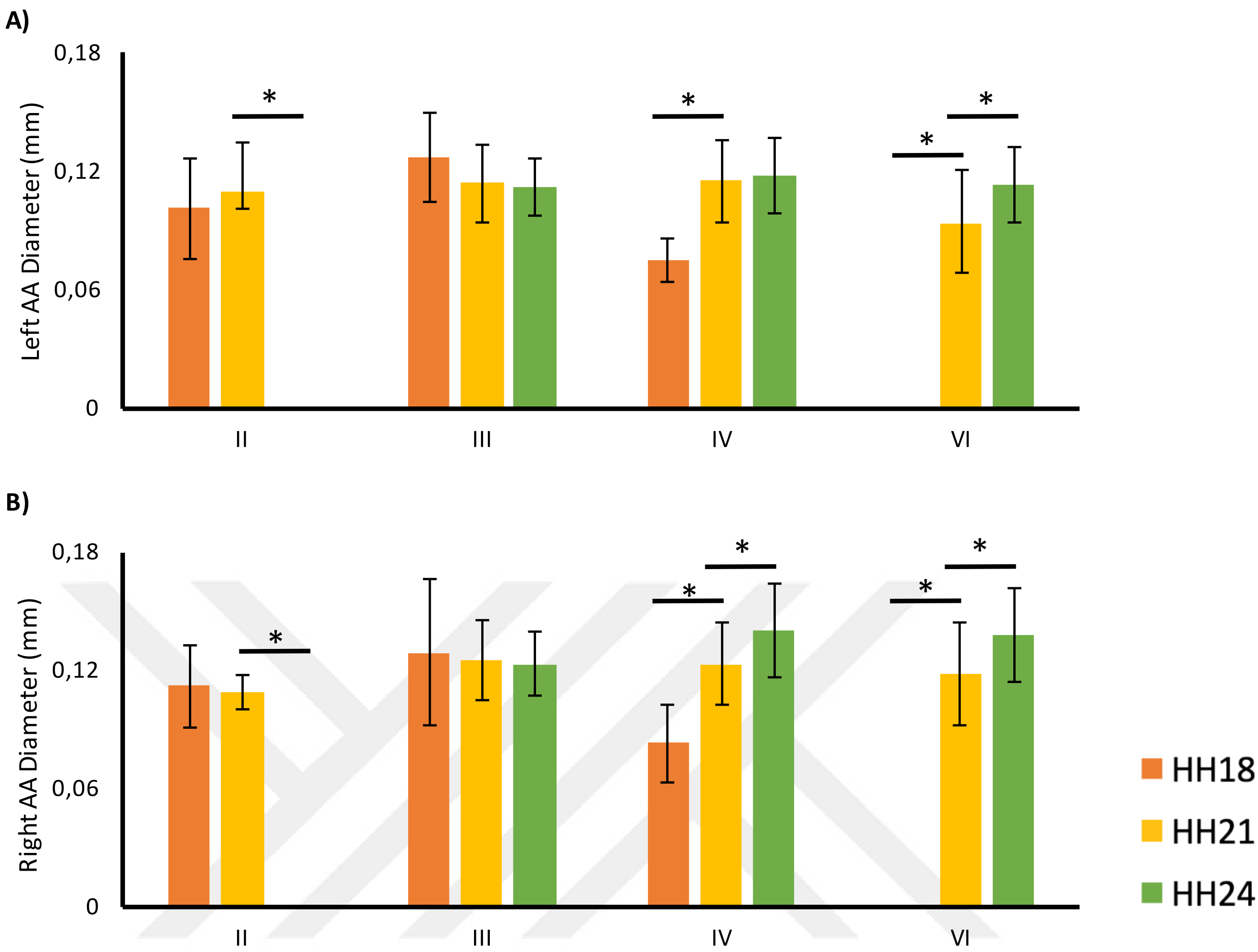

Figure 2.5 Individual diameters of left **(A)** and right **(B)** AA for HH18, HH21 and HH24 from our previous studies. Statistically significant differences within stages are indicated with * (p<0.05).

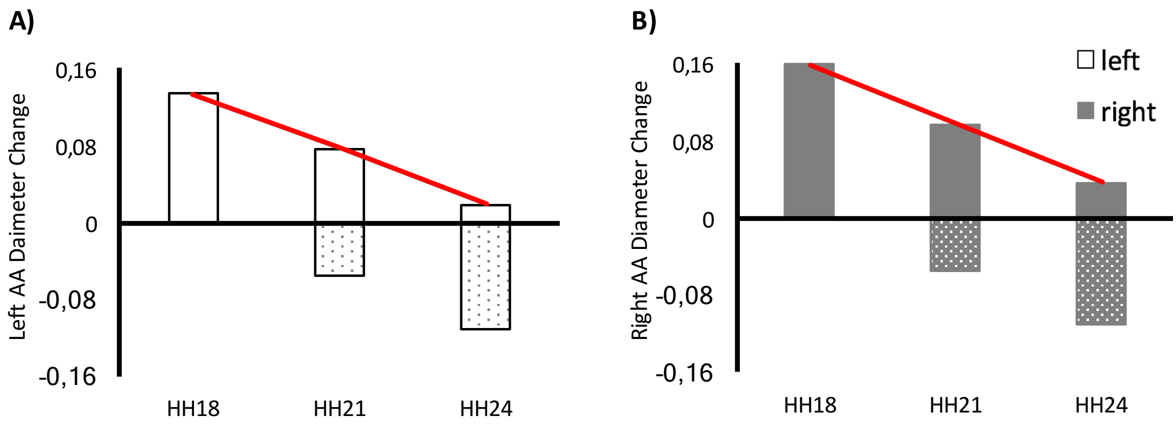

Figure 2.6 Significant diameter trend charts for left **(A)** and right **(B)** AA.

<u>Gene expression</u>

Angiogenesis genes

The expression level of *VEGF* continuously decreased for the right AAs from HH18 to HH21 ($p=0.002$), and then from HH21 towards HH24 ($p=0.01$) (Figure 2.7A). Similar decreasing trend was significantly observed for the left AAs from HH18 to HH21 ($p=0.024$). Left and right AAs, on the other hand, did not show any significant difference in their *VEGF* expression within the embryonic stages. *ANGPT1* expression (Figure 2.7B) significantly decreased towards HH21 in left AA ($p<0.001$) while expression increased in right AA ($p=0.017$). Left AA expression was higher than right AA expression at HH18 ($p<0.001$). *ANGPT2* expression (Figure 2.7C) significantly changed between all stages for right AA ($p<0.001$ for both) and decreased towards HH24 for left AA ($p=0,007$). Right AA expression was higher than left AA expression at HH18 ($p=0.004$) and HH21 ($p<0.001$). *CDH5* expression (Figure 2.7D) significantly increased ($p<0.001$ for left and $p=0.023$ for right) and then decreased ($p<0.001$ for left and right), while there was no change between left and right AA. *TGFβ2* (Figure 2.8A) expression gradually increased over time for both left ($p=0.022$ and $p<0.001$) and right AA ($p=0.001$ and $p<0.001$) with a significant left-right difference at HH24 ($p=0.033$). Although *TGFβ3* expression (Figure 2.8B) remained constant for left AA, expression increased towards HH21($p<0.001$) and decreased towards HH24 ($p<0.001$) in right AA with very low p values ($p<0.001$ for all). *MMP2* expression (Figure 2.8C) increased towards HH21 ($p<0.001$ for left and right) and became higher in left AA for HH24 ($p=0.008$). *TIMP3* expression (Figure 2.8D) was significantly changed for left AA ($p<0.001$ for both stages) and considerable left-right difference was seen at HH18 ($p=0.001$) and HH21 ($p<0.001$).

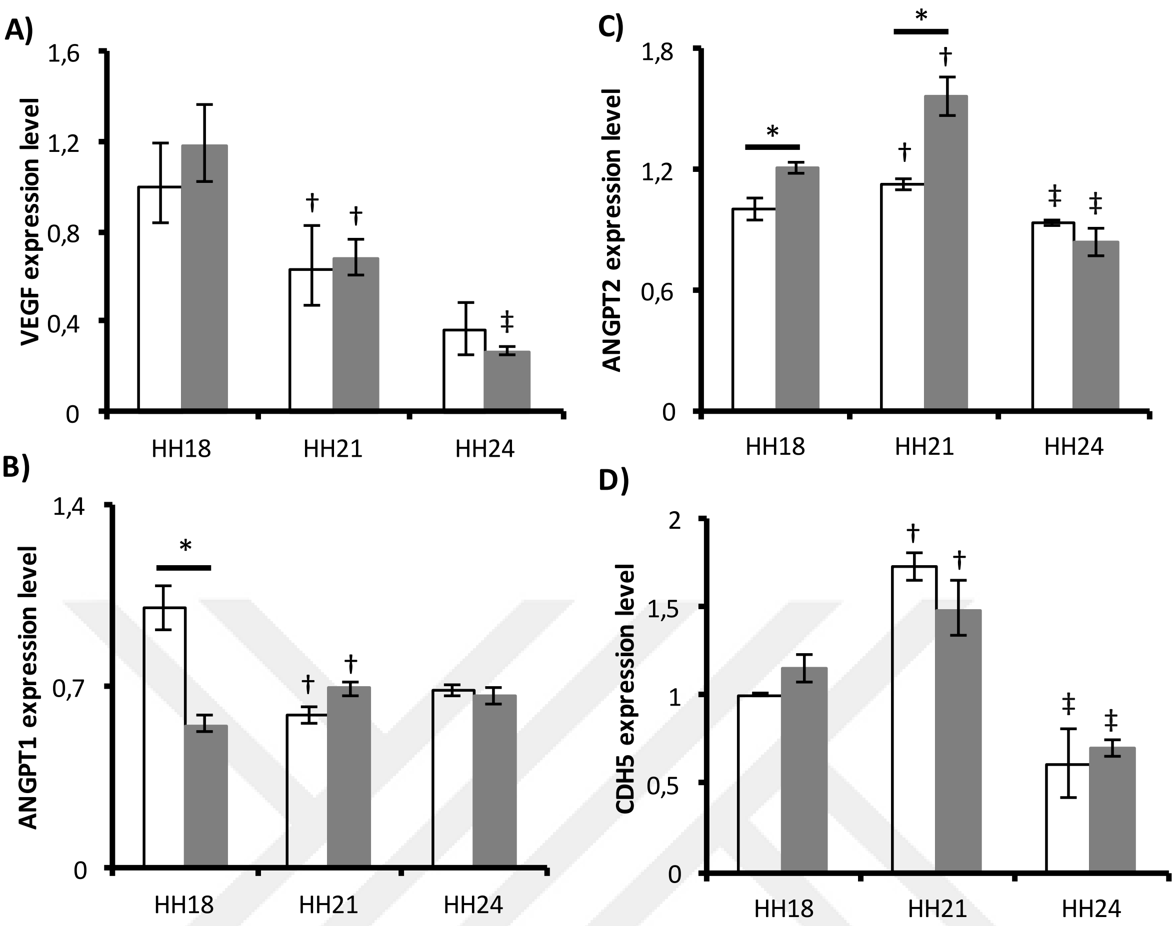

Figure 2.7 Expression levels of angiogenesis-related genes **(A)** VEGF **(B)** ANGPT1 **(C)** ANGPT2 **(D)** CDH5 for left and right AA at HH18, HH21 and HH24 were shown. GAPDH was used for normalization and fold changes were determined based on HH18 left AA. Following symbols indicate the statistical significant difference ($p<0.05$): † for difference in same side between HH18 and HH21; ‡ for difference in same side between HH21 and HH24; * for left and right AA differences within the same stage. (white: left AA, gray: right AA)

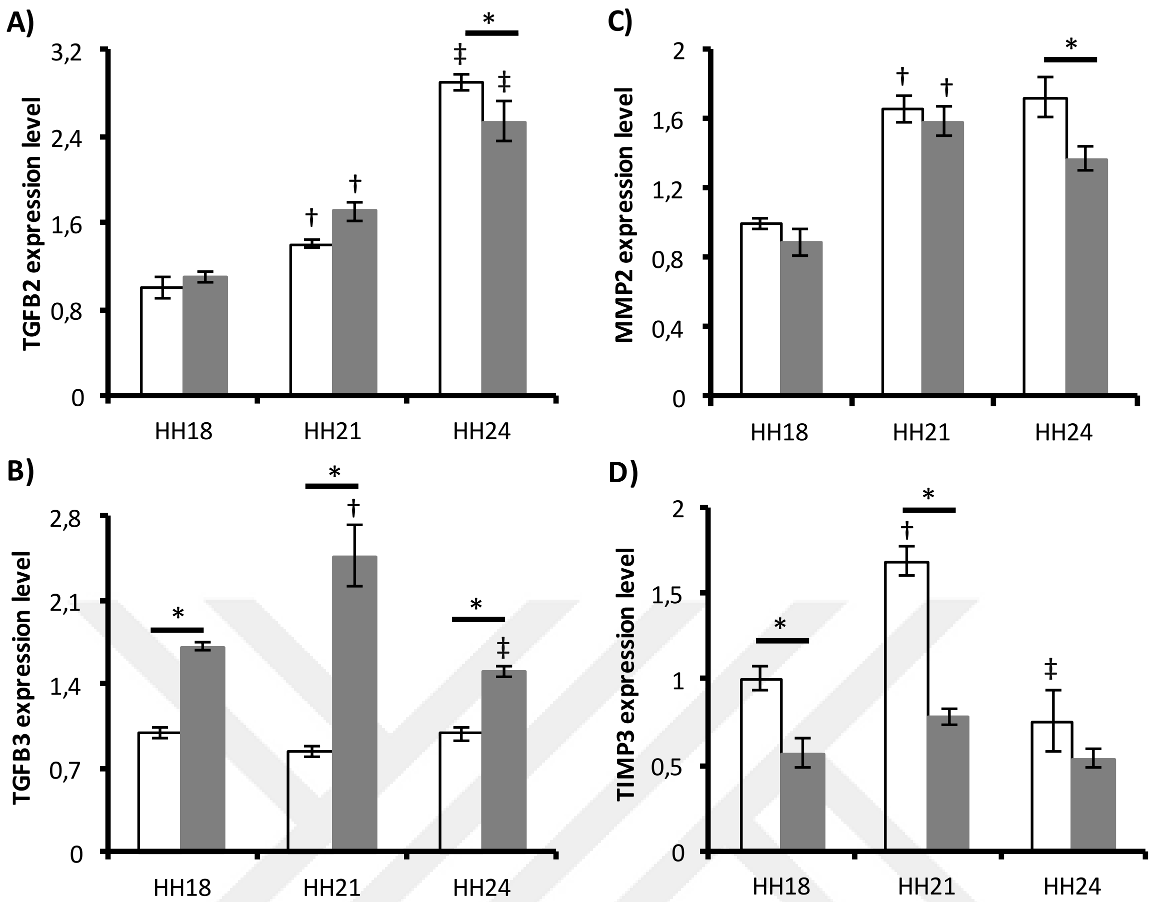

Figure 2.8 Expression levels of angiogenesis-related genes **(A)** TGFβ2 **(B)** TGFβ3 **(C)** MMP2 **(D)** TIMP3 for left and right AA at HH18, HH21 and HH24. were shown. GAPDH was used for normalization and fold changes were determined based on HH18 left AA. Following symbols indicate the statistical significant difference ($p<0.05$): † for difference in same side between HH18 and HH21; ‡ for difference in same side between HH21 and HH24; * for left and right AA differences within the same stage. (white: left AA, gray: right AA)

Cardiovascular development and remodeling genes

NOS3 expression (Figure 2.9A) significantly decreased from HH21 to HH24 (p=0.026 for left and p<0.001 for right) without any difference between left and right AA. *SHH* expression (Figure 2.9B) was significant for right AA with an increase from HH18 to HH21 followed by a decrease from HH21 to HH24 (p<0.001 for both). Right AA expression was higher for all stages. (p=0.041 at HH18, p<0.001 at HH21 and p=0.001 at HH24). *TBX1* expression (Figure 2.9C) significantly increased from HH18 to HH21 (p<0.001 for left and p=0.009 right) and decreased from HH21 to HH24 (p<0.001 for both left and right). Right AA expression was significantly higher at HH18 (p<0.001) while left AA expression was dominant at HH24 (p< 0.001). *FGF8* (Figure 2.9D) expression in AA gradually decreased during time. The decrease was significant between HH18 and HH21 (p<0.02 for left and p=0.040 for right), and left AA expression was significantly higher at HH18 (p=0.001). *ET1* expression (Figure 2.10A) also decreased with time. Significant decrease was observed from HH18 to HH21 (p=0.03 for left and p<0.001 for right) and from HH21 to HH24 (p=0.004 for left and p=0.002 for right). Moreover, left AA expression was higher at HH18 and HH21 (p<0.001 for both). For left AA, *HAND2* expression (Figure 2.10B) increased from HH18 to HH21 (p=0.001) with a following decrease from HH21 to HH24 (p=0.006). For right AA, *HAND2* expression increased from HH18 to HH21 and decreased from HH21 to HH24 (p<0.001 for both). Also, right AA expression was significantly higher at HH18 (p=0.028). *HOXA3* expression (Figure 2.10C) significantly increased only from HH21 to HH24 for left AA (p=0.008). Furthermore, left AA expression was significantly higher than right AA expression at HH24 (p=0.002). *HHEX* expression (Figure 2.10D) decreased over time with significant difference between HH18 and HH21 for right AA (p=0.005) and between HH21 and HH24 (p=0.001 for left and p<0.001 for right). Also, there was a significant change between left and right AA at HH24 (p<0.001).

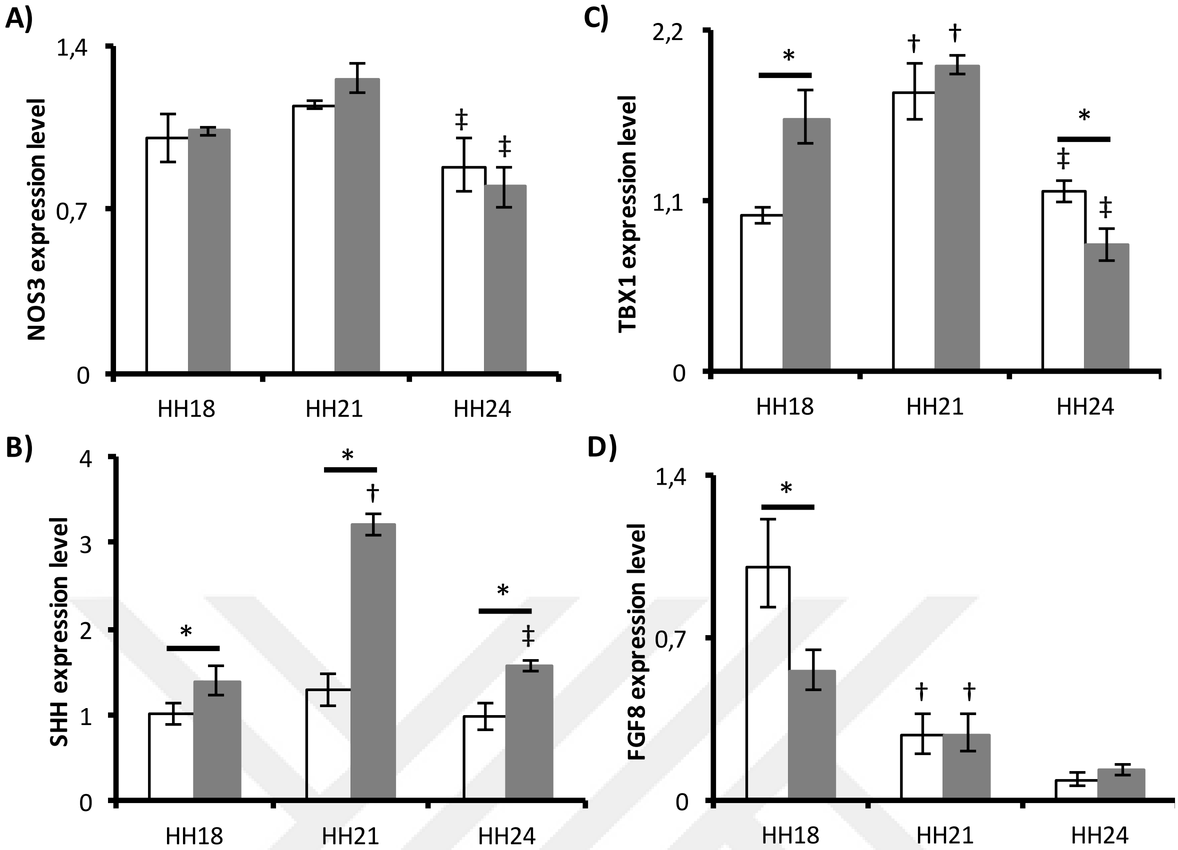

Figure 2.9 Expression levels of cardiovascular development and remodeling genes **(A)** NOS3 **(B)** SHH **(C)** TBX1 **(D)** FGF8 for left and right AA at HH18, HH21 and HH24 were shown. GAPDH was used for normalization and fold changes were determined based on HH18 left AA. Following symbols indicate the statistical significant difference ($p<0.05$): † for difference in same side between HH18 and HH21; ‡ for difference in same side between HH21 and HH24; * for left and right AA differences within the same stage. (white: left AA, gray: right AA)

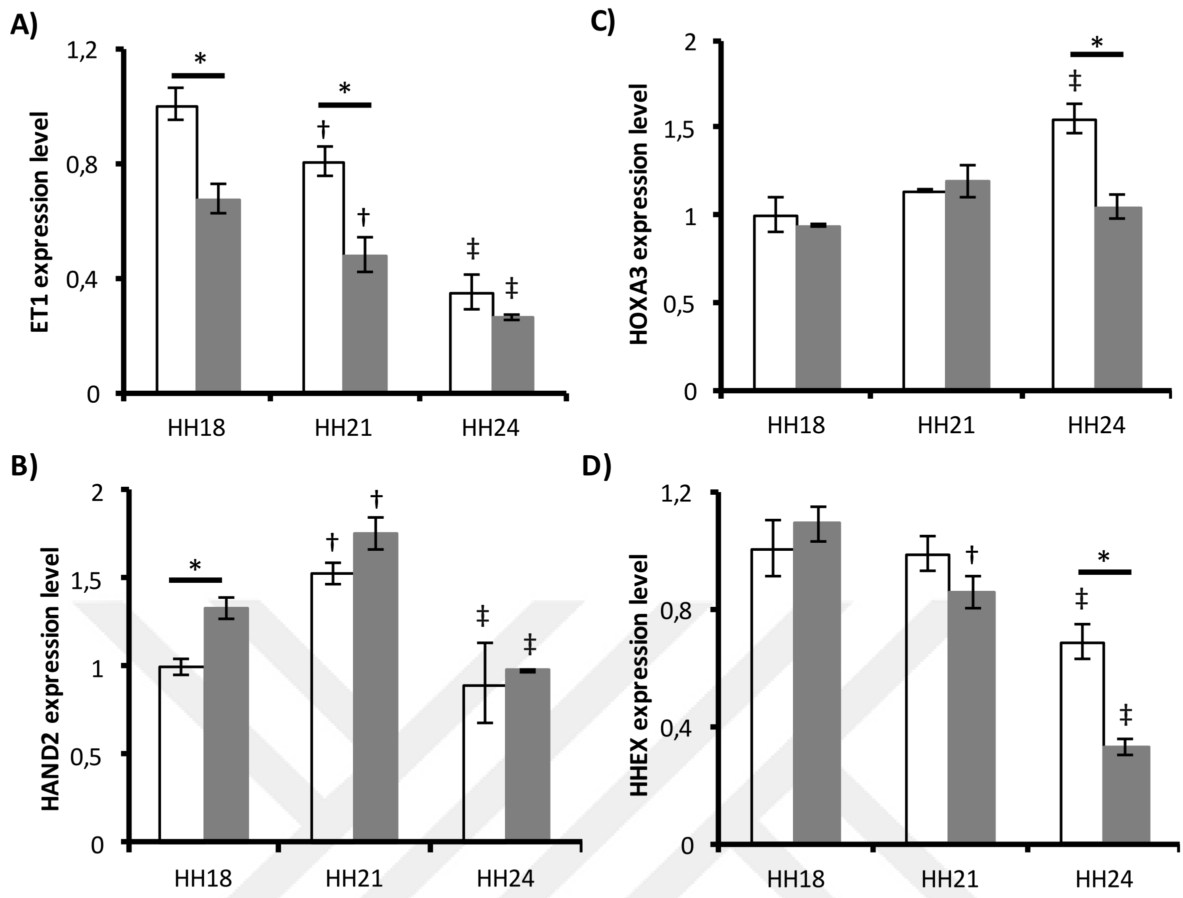

Figure 2.10 Expression levels of cardiovascular development and remodeling genes **(A)** ET1 **(B)** HAND2 **(C)** HOXA3 **(D)** HHEX for left and right AA at HH18, HH21 and HH24 were shown. GAPDH was used for normalization and fold changes were determined based on HH18 left AA. Following symbols indicate the statistical significant difference ($p<0.05$): † for difference in same side between HH18 and HH21; ‡ for difference in same side between HH21 and HH24; * for left and right AA differences within the same stage. (white: left AA, gray: right AA)

Extracellular Matrix, Cytoskeleton and Apoptosis genes

RT-qPCR analysis on the chick AAs showed *COL1* expression level increased significantly from HH18 to HH21 for both left ($p = 0.006$) and right ($p < 0.001$) AAs (Figure 2.11A). Unlike for stage HH18, left and right AAs were different noticeably ($p < 0.001$ and $p = 0.006$, respectively) within stages HH21 and HH24. *COL3* gene expression results indicated an up-regulation of this ECM protein in the right AAs from HH18 to HH21 and from HH21 to HH24 ($p < 0.001$ for both differences) (Figure 2.11B). Left AAs, on the other hand, showed significant variation between stages HH21 and HH24 ($p = 0.026$). Genetic expression for *COL4* by both right and left AAs increased significantly from HH18 to HH21 ($p = 0.001$ for left and $p = 0.002$ for right). Expression results for *COL4* revealed significant within-stage right and left side differences for all three stages ($p = 0.011$ for HH18, $p = 0.025$ for HH21, and $p = 0.041$ for HH24) (Figure 2.11C). *FN1* expression (Figure 2.11D) increased from HH18 to HH21 ($p<0.001$ for both left and right) and decreased from HH21 to HH24 ($p<0.001$ for left and $p=0.016$ for right). Right AA expression was significantly higher at HH24 ($p=0.001$). *FBN1* expression (Figure 2.11E) also significantly increased at first ($p=0.009$ for left and $p=0.001$ for right), and significantly decreased from HH21 to HH24 in right AA ($p=0.008$). *ELN* expression was significantly different for the right and left AAs at stages HH18 and HH21 ($p = 0.019$ for HH18 and $p < 0.001$ for HH21), whereas no such significance was observed for stage HH24 (Figure 2.11F). Left AAs' *ELN* expression first increased significantly from HH18 towards HH21 ($p = 0.012$), then indicated a decreasing trend towards HH24 ($p = 0.023$). Right AAs followed a similar trend with the left side during the same time course ($p < 0.001$ for both HH18-HH21 and HH21-HH24). Significant increase in *ACTA2* expression (Figure 2.12A) from HH18 to HH21 was seen in right AA ($p=0.013$), and a significant decrease from HH21 to HH24 was seen in both left ($p=0.002$) and right AA ($p=0.001$). *VCL* expression (Figure 2.12B) was significant in all stages. An increase in expression from HH18 to HH21 ($p<0.001$ for left and $p=0.006$ for right) was followed by a decrease from HH21 to HH24 ($p=0.007$ for left and $p=0.001$ for right). Expression in left AA was higher at all stages ($p=0.001$ at HH18, $p<0.001$ at HH21 and HH24). *CASP3* expression (Figure 2.12C) significantly increased in left AA from HH18 to HH21 ($p<0.001$). Also, right AA expression was higher at HH18 ($p=0.016$).

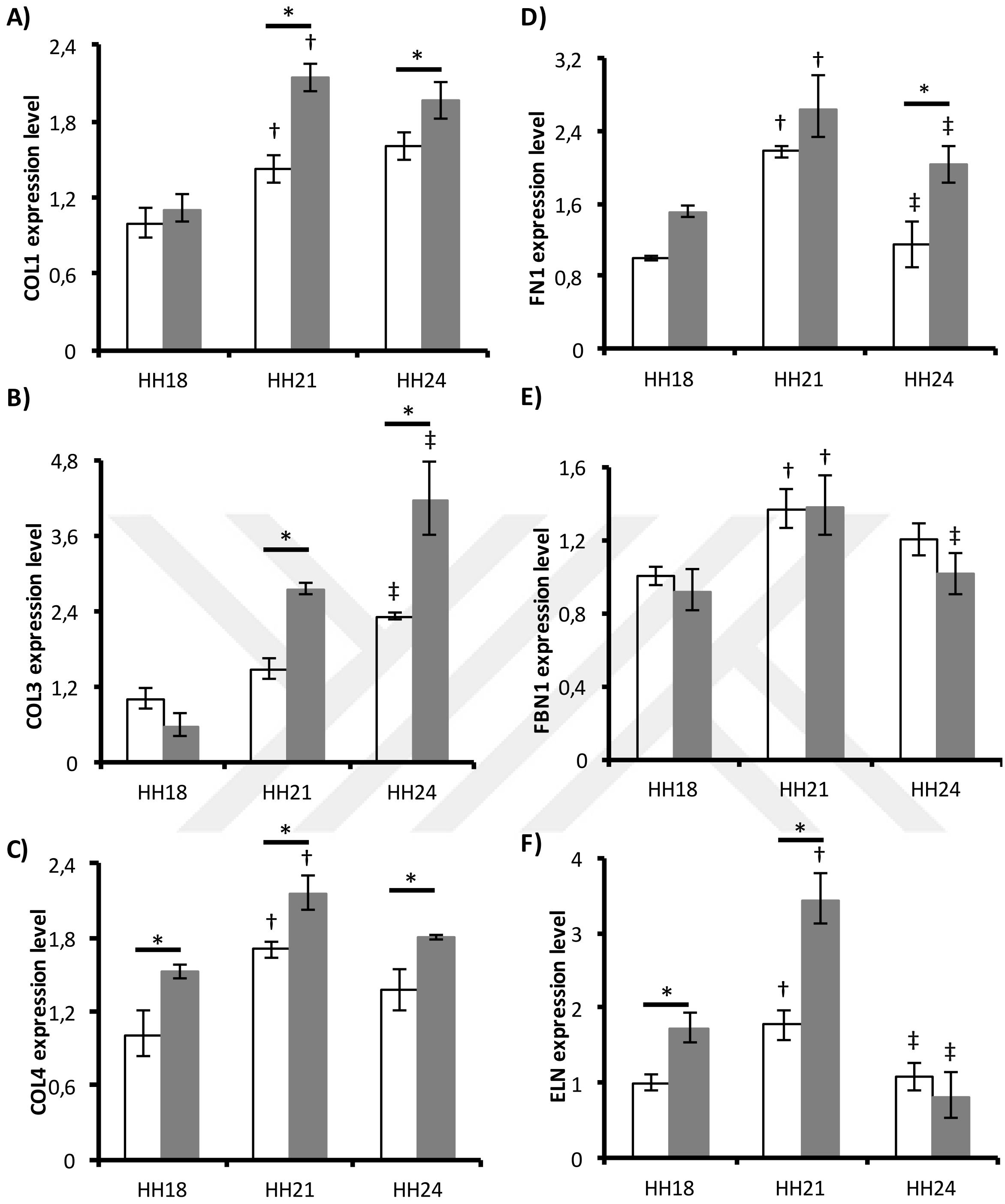

Figure 2.11 Expression levels of ECM genes **(A)** COL1 **(B)** COL3 **(C)** COL4 **(D)** FN1 **(E)** FBN1 **(F)** ELN for left and right AA at HH18, HH21 and HH24 were shown. GAPDH was used for normalization and fold changes were determined based on HH18 left AA. Following symbols indicate the statistical significant difference ($p<0.05$): † for difference in same side between HH18 and HH21; ‡ for difference in same side between HH21 and HH24; * for left and right AA differences within the same stage. (white: left AA, gray: right AA)

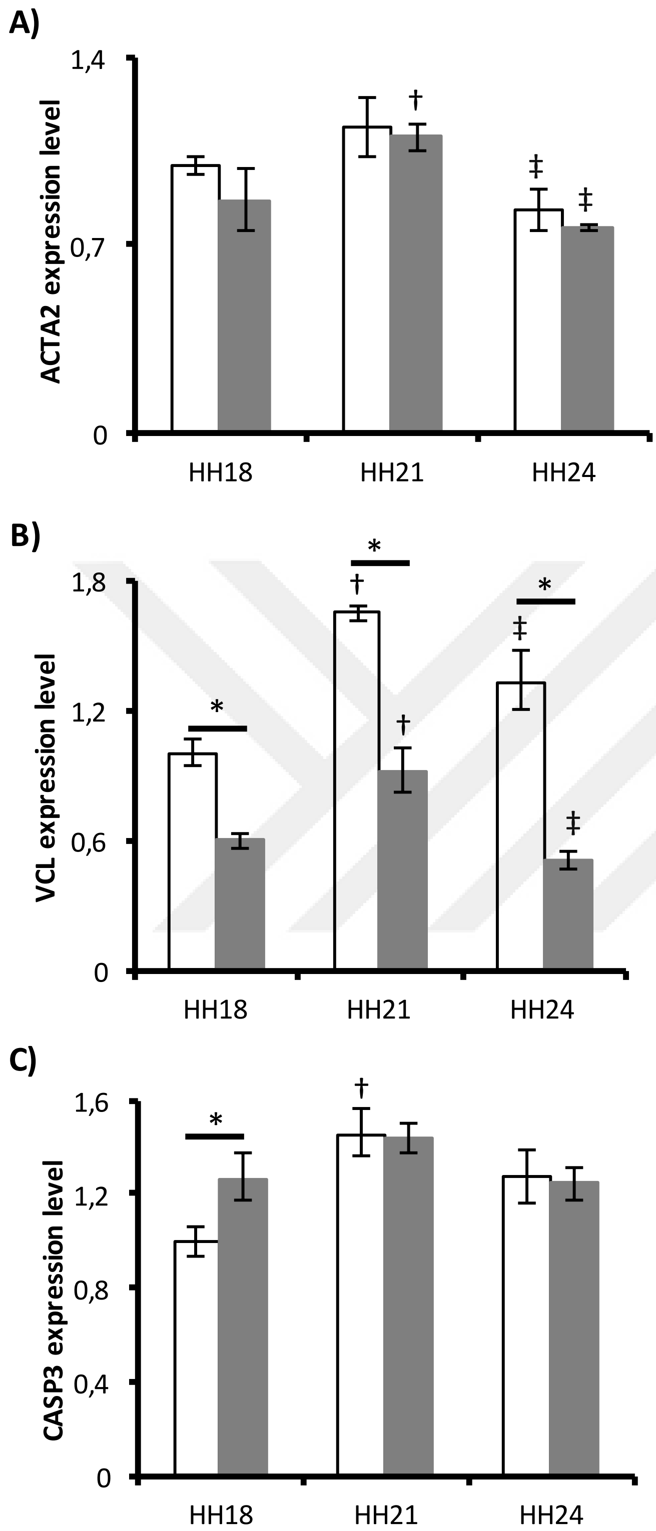

Figure 2.12 Expression levels of cytoskeleton and apoptosis-related genes **(A)** ACTA2 **(B)** VCL **(C)** CASP3 for left and right AA at HH18, HH21 and HH24 were shown GAPDH was used for normalization and fold changes were determined based on HH18 left AA. Following symbols indicate the statistical significant difference ($p<0.05$): † for difference in same side between HH18 and HH21; ‡ for difference in same side between HH21 and HH24; * for left and right AA differences within the same stage. (white: left AA, gray: right AA)

Correlation, peak expression and network development

Correlations for left and right AA were calculated based on the trends of the gene expressions. However, *HOXA3*, *MMP2* and *COL1* showed different trends on left and right AA, so they were grouped separately. Interestingly in this group of genes, left AA showed growth-trend and right AA showed WSS-trend, so they were correlated accordingly.

Most of the genes that we investigated were correlated strongly with averaged WSS. *FBN1* demonstrated the highest average R value of 0.973 among the WSS-correlated genes. The lowest correlation with WSS was seen in angiopoietins with average R values of 0.776 for *ANGPT1* and 0.758 for *ANGPT2*. Genes highly correlated with WSS were *FBN1, TGFβ3, SHH, VCL, CASP3, FN1, ELN, COL4, TIMP3, HAND2* and *TBX1*, in descending order. Genes with little correlation to WSS included *ACTA2, CDH5, NOS3, ANGPT1* and *ANGPT2*. Genes that were correlated with significant diameter change were *VEGF, FGF8, COL3, ET1, TGFβ2* and *HHEX*, in descending order. *VEGF* had the highest average R value of 0.9989 while *HHEX* R of 0.8947 was the lowest value.

Peak expression analysis was performed for WSS-correlated genes and the nodes of the network were aligned accordingly. Furthermore, the alignment within each column was arranged in descending order of correlation (Fig 7). The earliest peak expression in WSS-correlated genes was determined in *TBX1, ACTA2, CDH5* and *ANGPT2*. The next column included *HAND2* and *NOS3*. Third column included *TGFβ3, SHH, ELN* and *TIMP3*. *FN1* expression was determined later. *FBN1, VCL* and *CASP3* created another column while *COL4* and *ANGPT1* had the latest expression among all. Afterwards, genes with different left and right correlation trends (*HOXA3, MMP2* and *COL1*) were aligned to the network. The last group of the network was the growth-correlated genes, which were *VEGF-A, FGF8, COL3*, *ET1, TGFβ2* and *HHEX.*

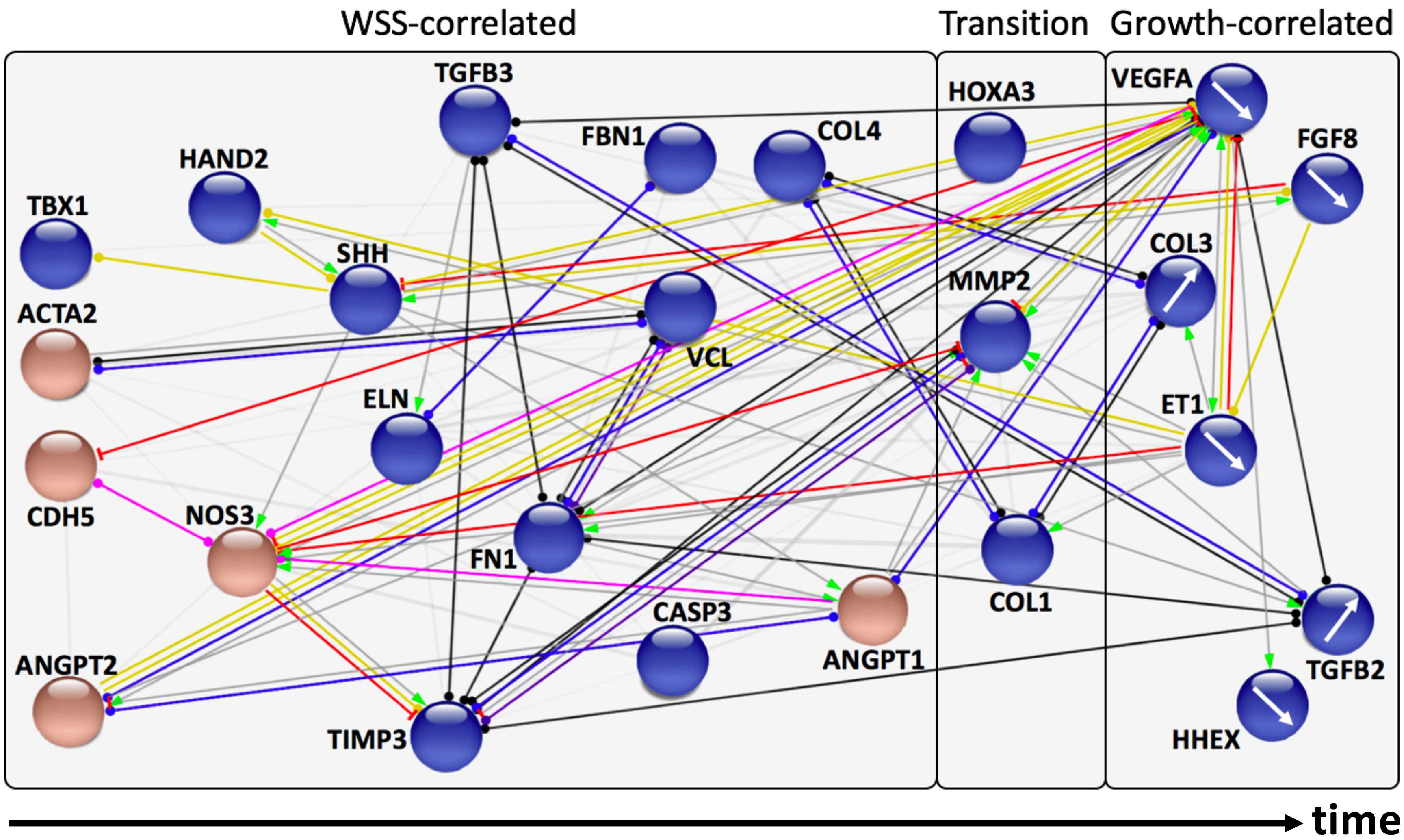

Figure 2.13 Temporal organization of the gene/protein network during AA morphogenesis. This network was constructed in association with the STRING database showing the selected molecular interactions between genes examined in this study, and aligned by time according to the corresponding correlations level (vertical axis) and peak expression times (horizontal axis). WSS-correlated, both WSS and growth-correlated (transition), and growth-correlated genes were aligned from left to right, respectively. Blue nodes show high correlation (R≥0.8) and brown nodes show low correlation (R<0.8). White arrows inside the nodes of growth-correlated genes show the trend of gene expression (steady increasing vs. steady decreasing expression). Colors of the edges represent the type of interactions listed next to the network. Directed arrow at the end of edges denotes positive effect, perpendicular line denotes negative effect, and circular shape denotes unspecified effect.

2.4 Discussion

Gene expression trends

Angiogenesis-related genes

Angiogenesis-related gene expressions other than *VEGF* and *TGFβ2* correlated well with the WSS-trend. Only left AA expressions of *ANGPT1* and *TGFβ3* showed inverse of the WSS-trend with a decrease through HH21 following an increase. Other genes in this pathway, including the right AA expressions of *ANGPT1* and *TGFβ3* followed the regular WSS-trend.

Angiopoietins are important regulators of vascular activation, remodeling and angiogenesis [25] together with VEGF [26]. ANGPT1 is required for embryonic vascular development and ANGPT2 takes role in vascular remodeling by controlling the functioning of other angiogenic proteins [25]. According to the prevailing model of vascular development, VEGF forms the immature vasculature, and ANGPT1 further remodels and matures the initial vasculature. Moreover, ANGPT1 maintains the stability and quiescence of the vessels while ANGPT2 destabilizes the vessels and promotes sprouting in the presence of VEGF and regression in the absence of VEGF [26]. According to our results, *VEGF* expression decreases for left and right AA through development. *VEGF* expression is much more needed during vasculogenesis; thus, its level should decrease in later stages. Still, it is required for angiogenic processes, and its highest expression at HH18 might be the indicator of sprouting between HH18 and HH21 stages. In addition, left AA expression for *ANGPT2* directly follows the WSS-trend while that of *ANGPT1* inversely follows the WSS-trend. Therefore, ANGPT2 level is higher in left AA, which implies that the left lateral AA are more unstable than the right. This behavior can be a cue for the eventual right-sided aortic arch preference in the chick embryos.

Table 2.2: Literature review and compatibility of gene expression trends with shear stress

Gene	Model organism	Shear stress type	Compatibility with our results	Reference
ANGPT1	Human Umbilical Vein EC	LSS	NO	[27]
	Mice mature AA	LSS and OSS	NO	[28]
ANGPT2	Human Umbilical Vein EC	LSS	NO	[27]
	Human Umbilical Vein EC	LSS	NO	[29]
	Human Aortic EC	LSS and OSS	YES	[30]
	Human Umbilical Vein EC, Mice mature AA	LSS and OSS	YES	[28]
CDH5	Porcine aortic EC	LSS	YES	[31]
	Endothelial precursor cells	LSS	YES	[32]
TGFβ2,3	Mice Embryonic EC	LSS	YES	[33]
NOS3	Human Umbilical Vein EC	LSS and PSS	YES	[34]
	Chick RVA	Physiological	YES	[19]
	Chick AA	Physiological	YES	[20]
ET1	Bovine Aortic EC	LSS, PSS, TSS	YES	[35]
	Chick RVA	Physiological	YES	[19]
	Chick AA	Physiological	NO	[20]
ACTA2	Porcine aortic Valve EC	LSS and OSS	YES	[36]
VCL	Bovine Aortic EC	LSS	YES	[37]
	Human Umbilical Vein EC	PSS	YES	[34]

* LSS: steady laminar shear stress; OSS: oscillatory shear stress; PSS: pulsatile shear stress; TSS: turbulent shear stress.

ANGPT2 is shear stress regulated. *ANGPT2* mRNA expression was reported to decrease under dynamic conditions [27] and low laminar flow upregulated *ANGPT2* mRNA and protein expression while high flow downregulated this gene [29]. However, *ANGPT2* expression was upregulated by the oscillatory shear stress (OSS) and pulsatile shear stress (PSS) *in vitro* and *in vivo* [28, 30]. In our experiments, we also observed that *ANGPT2* expression was positively correlated with WSS both for left and right AA. Therefore, it can be concluded that OSS and PSS regulations are partly responsible for the changes in *ANGPT2* expression in AA.

Vascular endothelial cadherin (VE-cadherin/*CDH5*) is one of the most critical adhesive molecules spanning the membrane and transferring the information to intracellular compartments in cell-cell junctions [38, 39]. It is required for angiogenesis and vascular morphogenesis [40]. As such, it is a part of a mechanosensory complex that senses shear stress [41]. Studies showed that CDH5 levels were increased with shear stress in porcine aortic EC [31]. Furthermore, shear stress increased CDH5 protein and mRNA expression level in endothelial progenitor cells [32]. Our results also showed the same WSS pattern for *CDH5* expression conforming its role of shear sensing and transducing in chick embryonic AA.

TGFβ signaling plays a significant role in angiogenesis, cardiovascular development and remodeling systems by regulating cellular processes such as cell growth, proliferation, migration, differentiation and even apoptosis [42, 43]. In addition, TGFβ signaling enhances the expression of SMC proteins and matrix proteins such as fibronectin, collagen and elastin [11]. During embryogenesis, TGFβ2 plays role in the development of AA IV [44]. Studies on the remodeling of AA show that *TGFβ2* knockout mice develop hypoplasia and interruptions in AA IV, whereas *TGFβ3* knockout mice has minor changes in curvature of AA without being lethal [45]. In one study, mouse embryonic EC were exposed to shear stress, and it was seen that *TGFβ3* expression increased with shear stress while *TGFβ2* expression was unchanged. This result also explained the difference in cross-talk between embryonic and adult ECs [33].

We also recorded that *TGFβ3* expression followed the WSS-trend and *TGFβ2* expression did not, which is in correlation with the findings of Egorova *et al.* [33] Furthermore, constant increase in TGFβ2 might stem from the further maturation of the ECM proteins during later stages.

MMPs are important regulators of angiogenesis by degrading the vascular basement membrane and ECM components [46]. On the other hand, tissue inhibitor of matrix metalloproteinases (TIMPs) inhibits the MMP activity, thereby inhibiting angiogenesis. *TIMP3* expression can be induced by shear stress via ETS-1 mediated pathway [47]. Our results also show that *TIMP3* expression was regulated with WSS. In addition, MMP2 activates latent TGFβ2 during angiogenesis [46]. For both left and right AA, *MMP2* expression significantly increased from HH18 to HH21. This increase might indicate the angiogenic events in transition from HH18 to HH21. In addition, mechanical stress is known to activate some intracellular pathways which eventually stimulates *MMP2* expression [48]. WSS may also be the reason in the upregulation of *MMP2* through HH21.

Cardiovascular Development and Remodeling Genes

In this group of genes, a WSS-related trend was observed in *NOS3, TBX1, HAND2* and *SHH* expressions. Gene expressions for *ET1, HHEX* and *FGF8* followed growth-trend inversely while *HOXA3* expression had different trends for left and right AA.

Endothelial nitric oxide synthase (NOS3) is expressed in EC, and has a variety of roles including vasodilation, controlling blood pressure and controlling SMC proliferation [49]. It is well established that *NOS3* is a shear stress responsive gene. In vitro studies demonstrate that *NOS3* expression is upregulated with laminar and unidirectional PSS [34]. Indeed, *NOS3* responds the WSS change relatively fast and reversibly [19]. In addition, *NOS3* expression is seen in the narrow parts of cardiovascular system where WSS is high. However, *NOS3* expression remains stable in AA of chick embryos [20]. Our results confirm the observations of Groenendijk *et al.* *NOS3* expression in left and right AA followed WSS-trend as expected, but a significant change between different stages were not captured *in vivo*.

Sonic hedgehog signaling pathway is one of the most crucial regulators of cell differentiation and cell proliferation. The most expressed ligand of this pathway, sonic hedgehog (SHH), has significant roles in embryonic development [50], particularly, cardiovascular and pharyngeal arch development [51]. *SHH* mutant embryos have abnormal AA development and abnormal pathways for neural crest cell migration [51]. T-box transcription factor-1 (TBX1) has roles in AA formation and early remodeling [52]. Heterozygous mutation in *TBX1* gene causes reduction or complete absence of AA IV while the mutation in both copies disrupts the whole AA system [53, 54]. It was found that TBX1 functions as downstream of SHH in pharyngeal arch development [55]. This interaction can be seen in right AA where *TBX1* and *SHH* expression have significantly altered WSS-trend. Fibroblast growth factor-8 (FGF8) is another molecule necessary for pharyngeal arch and cardiovascular development. Hypomorphic mutation of *FGF8* causes several AA development defects in mouse embryos including hypoplasia or complete absence of AA IV which eventually results in aortic arch and subclavian artery defects in adults [56, 57]. It was found that *TBX1* and *FGF8* genetically interact in the AA development, and *TBX1* functions upstream of *FGF8* [58]. Moreover, specific ablation of *TBX1* in pharyngeal endoderm showed that *FGF8* expression was reduced in that region supporting the earlier findings [59]. Our data showed that *TBX1* followed WSS-trend while *FGF8* expression followed inverse growth-trend for both left and right AA. The highest expression of *FGF8* was at HH18 while peak expression of *TBX1* in left AA was at HH21 and right AA was between HH18 and HH21. Therefore, the interaction between *TBX1* and *FGF8* might have a time-lag in patterning of aortic arch. In addition, the role of TBX1 in AA IV development is cell non-autonomous [60], meaning that *TBX1* is not expressed in the components of the vessel itself, but expressed in the pharyngeal endoderm. In our results, we observed the WSS-trend in *TBX1* expression. Thus, EC lining the AA sense WSS and might induce a signaling cascade eventually activating *TBX1* expression in pharyngeal endoderm.

Endothelin-1 (ET1) is a peptide having roles in cardiovascular development including AA remodeling and patterning [61]. Homozygous mutation of *ET1* results the persistence of AA I and II, and hypoplasia of AA IV [62]. It is known that ET1 is shear responsive in such a way that *ET1* mRNA and peptide expression were downregulated with both steady and pulsatile shear stress [35]. Moreover, Groenendijk *et al.* stated that high shear stress areas have lower *ET1* expression [20]. They also semi-quantitatively represented that *ET1* expression in AA increased during development of chick embryos, and assumed that shear stress in AA decreased due to the widening of the lumen. Our results showed that WSS increased in AA with a peak at HH21, and *ET1* expression decreased through HH24 for both left and right AA. This result is in correlation with our previous studies of *ET1* expression in RVA of chick embryos, stating that *ET1* expression decreased with increasing shear stress, and affected by the delay between shear and pressure [19]. Although TBX1 is not related with endothelin signaling in the morphogenesis of AA [63], FGF8 is related in such a way that *FGF8* is the upstream of *ET1* expression in the ectodermal signaling of the first pharyngeal arch [64]. Our results show that *FGF8* and *ET1* expression followed the same decreasing trend, which might be a clue for their relation in AA. *dHAND* or *HAND2* is expressed in the mesenchyme of the branchial arches and neural-crest derived structures in the developing heart [65]. HAND2, required for the survival of neural crest cells in AA, is stimulated by epithelial signaling of ET1, and this signaling cascade regulates the patterning of AA [66]. Mice homozygous mutant for *HAND2* had involute AA and eventually die [67]. We did not observe any relation between the expressions of *HAND2* and *ET1*, but probably our time scale is late for observing this kind of interaction since the neural crest cell migration is completed by HH18. Our results showed that *HAND2* expression followed WSS-trend for both left and right AA, but the mechanism to induce this expression should be further investigated.

HOXA3 plays a critical role in the development and differentiation of the third pharyngeal arch [68]. In addition, *HOXA3* null mutants have degenerated AA III which eventually results in common carotid artery defects [69]. *HOXA3* expression only showed a significant increase between HH21 and HH24 in left AA. This non-significant change might be explained with the existence of AA III at all the stages. Hematopoietically expressed homeobox gene (*HHEX*) is the early marker of EC during embryogenesis [70]. It is required for the differentiation of endothelial and hematopoietic lineages [71]. In addition, *in vitro* results showed that it acts as a negative regulator of angiogenesis [72]. Our results showed that its expression decreased through development while the expression patterns of other angiogenic molecules increased which might support the work of Nakagawa *et al.* Furthermore, the decrease in *HHEX* expression makes sense since it is required early in development.

Extracellular Matrix, Cytoskeleton and Apoptosis Genes

All ECM genes other than *COL1* and *COL3*, cytoskeleton and apoptosis-related genes followed the WSS-trend.

Transcription of the *COL1* did not vary significantly between stages HH21 and HH24, indicating that the most critical microstructural and macromolecular changes affecting the synthesis of this protein occurred mainly between stages HH18 and HH21. COL3 synthesis, on the other hand, significantly increased between HH21 and HH24 for both laterals of AA. In a previously published work, the appearance of Type-III collagen was detected later than the occurrence of COL1 and COL4 during avian embryogenesis [73]. Our results on gene expression and time-lapsed network analysis may confirm this relationship between COL1 and COL3.

COL4, as the only non-fibrillar collagenous protein investigated in our study. *COL4* expression in the right- and left-sided tissues significantly increased from HH18 to HH21 (2.16 fold, and 1.7fold, respectively). Notably, for each stage, COL4 mRNA levels were significantly higher for the right side. Again, the higher amounts of COL4 which give stability in right AA might be associated with the formation of right-sided mature aortic arch in later stages.

Fibronectin is an extracellular glycoprotein and has major roles in vascular development, growth and migration of EC and SMC and ECM remodeling [74]. In addition, presence and the stability of fibronectin provides the deposition of several ECM molecules including Collagen I and III, and influence the cell behavior [75]. Our data showed that fibronectin gene (*FN1*) expression followed WSS-trend with significant changes. Moreover, the notable change in the expression of *COL1* between HH18 and HH21 for left and right AA might be related to the change in *FN1* expression. Also, *COL3* showed an increasing trend which might show the further deposition of this protein [76].

Although production of elastin within the AAs during the later stages increased with the incubation period, its synthesis decreased from HH21 towards HH24 due to the instabilities. At the earlier stages, the elastin protein is not firmly cross-linked to ECM as the aortic elastin at later stages of development [77].Thus, this may create unstable response of elastin synthesis in early stage embryos. On the other hand, more studies have been conducted on the elastin synthesis in late stage embryos. One of those studies showed that the elastin fibers in the embryonic aorta became more conspicuous following ED 9 suggesting a gradual increase in elastin synthesis as the embryo mature [78]. Tokimitsu *et al* reported a gradual decrease in the mRNA expression of the elastin in the aorta of a mature chick embryo from ED12 to ED21[79]. Our results on Tropoelastin (*ELN*) mRNA distribution also revealed that both the right- and left-sided tissue sections expressed higher levels of *ELN* mRNA for stage HH21 compared to HH18 suggesting that the increased ELN synthesis within the vessel wall AAs might have contributed to the increased elastogenic activity in these tissue sections.

Fibrillin, another ECM protein, is the building blocks of microfibrils which eventually form the elastic fibers of the cell. Fibrillin provides a scaffold for elastin assembly by binding ELN monomers. Fibrillin-1 gene (*FBN1*) showed an expression pattern similar to elastin in the development of the mouse aorta [80]. Our results also showed that *FBN1* expression was similar to that of *ELN* expression which follows WSS-trend [76].

Smooth muscle alpha actin (ACTA2) is responsible for the contractile function of vascular SMC [81]. Previous work has shown that *ACTA2* expression was upregulated in the porcine aortic valve EC with the exposure to OSS [36]. The same is valid for its expression in AA. Vinculin (VCL) is an adapter protein which binds actin filaments to integrins in cell-matrix adhesion and to cadherins in cell-cell adhesions [82]. It was demonstrated that VCL functioned in the alignment of the stress fibers in response to shear stress [37]. Moreover, *VCL* expression was upregulated with prolonged unidirectional pulsatile flow [34]. Recent evidence suggests that VCL also functions in mechanoregulation of VE-cadherin [83]. Our results confirmed the effect of WSS on *VCL* expression and might show the interaction between VCL and VE-cadherin.

During the normal development of vessels, regression of the existing vessels is important as well as the formation of the new ones. The process is controlled by the balance between proliferation and apoptosis of EC [84]. Caspase-3 is the main protein involved in the apoptosis of existing vessels [85]. We thought that Caspase-3 might have a role in the disappearance of AA II in the transition from HH18 to HH21. We saw a significant increase in *CASP3* expression in the left AA between HH18 and HH21 but did not see the same result in right AA. Since the whole lateral arch tissue was collected and examined, as a limitation, we might not detect the individual changes within each AA vessel.

Time-lapsed Network Analysis

Hemodynamic changes in the vessels alter the activity of the cells. In particular, the cells lining the vessels sense WSS, and react to this biomechanical stress by changing their proliferation, alignment and apoptosis patterns. In the light of these, we hypothesized that genes correlated with WSS should be activated earlier, and affect the expression of growth-correlated genes. Thus, the locations of the genes in the network were organized accordingly based on their peak expression times. In this temporal network, it was seen that the growth factors VEGF and FGF8 were downregulated with the signals coming from WSS-correlated genes. In addition, TGFβ2 was upregulated which might be due to the need of ECM proteins for further development. In general, the structural genes such as collagens were activated relatively later than cardiovascular development and remodeling genes, so those genes likely influence the genes responsible for generating the structural components of the vessels. This time-resolved network approach can help predict the expression patterns of critical genes that are not included in the present investigation. For instance, *PITX2* gene plays a critical role in the left-right asymmetric morphogenesis of AA [16]. In the network, PITX2 is related with FGF8, which has an inhibitory effect (Supplemental Fig 2). *FGF8* expression decreases during AA development, thus *PITX2* expression is likely to increase and promote asymmetry in AA apparatus. SMAD2 plays a critical role in signal transduction initiated by TGFβ to promote the expression of matrix proteins [11]. *TGFβ2* expression increases through HH24 in AA, so *SMAD2* expression is expected to increase since TGFβ2 is shown to activate SMAD2 in network. The predictive capability of this time-resolved network approach needs to be confirmed through further validation experiments.

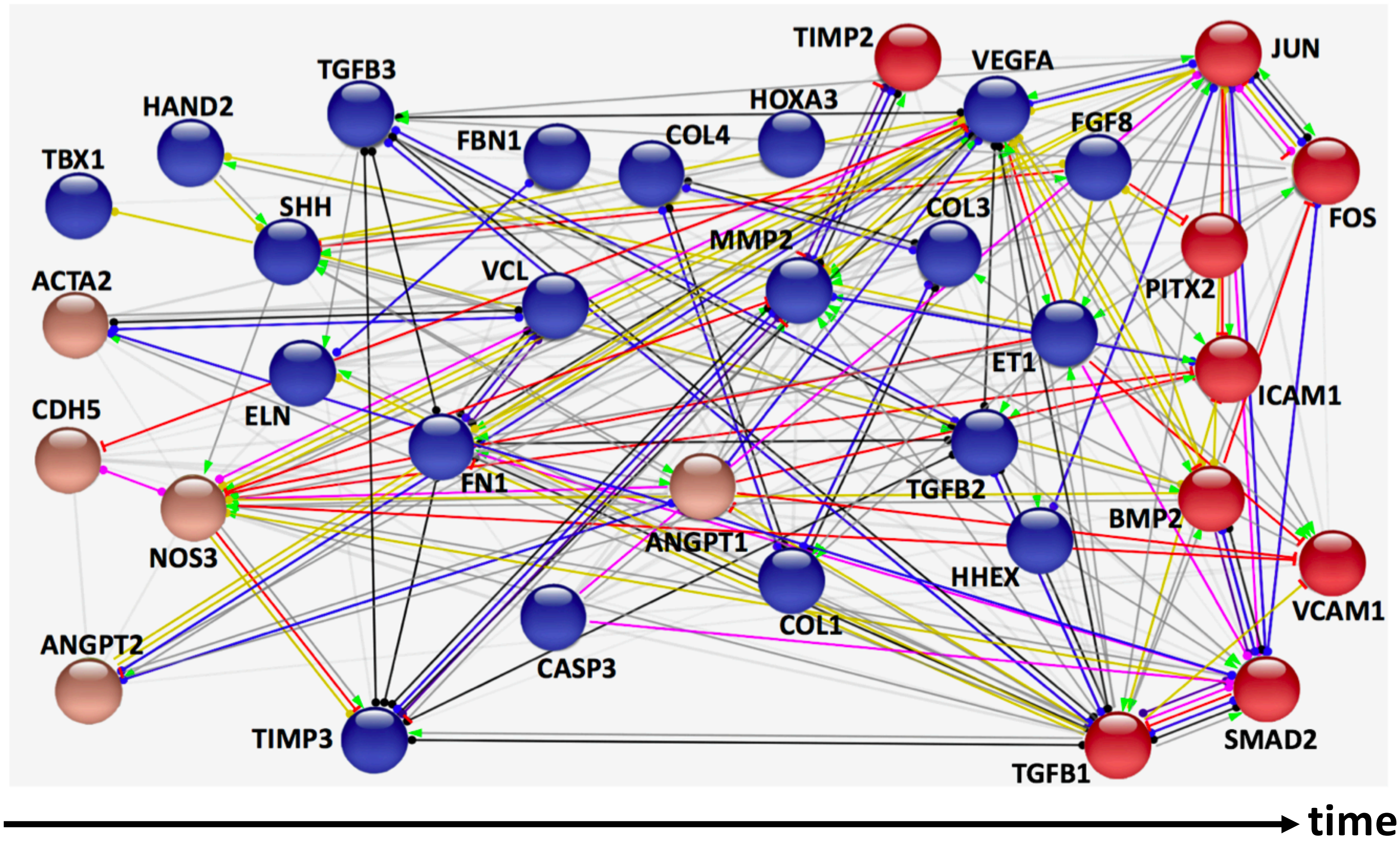

Figure 2.14 Gene/protein network for prediction. Including selected genes (*TIMP2, JUN, FOS, PITX2, BMP2, ICAM1, VCAM1, SMAD2, TGFβ1*) with unknown temporal expression patterns enriches the network constructed in Figure 2.13. Network was taken from STRING showing the molecular interactions between genes examined in this study, and aligned by time according to the correlations and peak expressions. WSS-correlated, both WSS and growth-correlated (transition), and growth-correlated genes were aligned from left to right, respectively. Blue nodes show high correlation ($R \geq 0.8$), brown nodes show low correlation ($R < 0.8$) and red nodes show the genes whose activity can be predicted. Colors of the edges represent the type of interactions listed next to the network (green=activation, red=inhibition, blue=binding, black=reaction, yellow=transcriptional regulation, pink=posttranslational modification, purple=catalysis, gray=unspecified). Directed arrow at the end of edges denotes positive effect, perpendicular line denotes negative effect, and circular shape denotes unspecified effect.

Chapter 3. Conclusion and Future Work

Aortic arch morphogenesis is a critical process in the global cardiac morphogenesis and errors result in and occur coincident with congenital heart diseases. The biological pathways controlling the development and the morphogenesis of AA are regulated with hemodynamic alterations. WSS has a significant effect on the expression of genes regulating different biological pathways in the AA morphogenesis of chick embryos, particularly in angiogenesis, vascular structure and apoptosis-related genes. A comprehensive analysis of fundamental trends was presented with varying levels of symmetry breaking. Peak expression analysis and novel time-resolved network maps were constructed that allowed the integration of WSS response with the regulatory growth-related gene expression pattern, particularly the growth factors. This novel network approach was the first-step towards predictive computational mechanogenomic models where interaction between the genetic characteristics and the resulting morphology can be estimated for more complex diseased conditions and models.

References

1. Gilbert, S.F., *Lateral Plate Mesoderm and Endoderm*, in *Developmental Biology*. 2010, Sinauer Associates, Inc.: Sunderland, USA. p. 445-498.
2. Kirby, M.L., *Vascular Development*, in *Cardiac Development*. 2007, Oxford University Press: New York, USA. p. 9-20.
3. Carmeliet, P., *Mechanisms of angiogenesis and arteriogenesis.* Nat Med, 2000. **6**(4): p. 389-95.
4. Mascio, C.E. and E.H. Austin, *Vascular Rings, Slings and Other Arch Anomalies*, in *Mastery of Cardiothoracic Surgery*, L.R. Kaiser, I.L. Kron, and T.L. Spray, Editors. 2014, Lippincott Williams & Wilkins: Philadelphia, USA. p. 797-815.
5. Congdon, E.D., *Transformation of the aortic-arch system during the development of the human embryo.* Contributions to Embryology, 1922. **277**(14): p. 47-110.
6. Seidelmann, S.B., J.K. Lighthouse, and D.M. Greif, *Development and pathologies of the arterial wall.* Cell Mol Life Sci, 2014. **71**(11): p. 1977-99.
7. Roman, B.L. and K. Pekkan, *Mechanotransduction in embryonic vascular development.* Biomech Model Mechanobiol, 2012. **11**(8): p. 1149-68.
8. Yashiro, K., H. Shiratori, and H. Hamada, *Haemodynamics determined by a genetic programme govern asymmetric development of the aortic arch.* Nature, 2007. **450**(7167): p. 285-8.
9. Hogers, B., M.C. DeRuiter, A.C. Gittenberger-de Groot, and R.E. Poelmann, *Unilateral vitelline vein ligation alters intracardiac blood flow patterns and morphogenesis in the chick embryo.* Circ Res, 1997. **80**(4): p. 473-81.
10. Groenendijk, B.C., K. Van der Heiden, B.P. Hierck, and R.E. Poelmann, *The role of shear stress on ET-1, KLF2, and NOS-3 expression in the developing cardiovascular system of chicken embryos in a venous ligation model.* Physiology (Bethesda), 2007. **22**: p. 380-9.
11. Gittenberger-de Groot, A.C., M. Azhar, and D.G. Molin, *Transforming growth factor beta-SMAD2 signaling and aortic arch development.* Trends Cardiovasc Med, 2006. **16**(1): p. 1-6.
12. Hamburger, V., Hamilton, H.L., *A series of normal stages in the development of the chick embryo.* J Morphol, 1951 **88**: p. 49-92.
13. Stanton, L.W., *Methods to profile gene expression.* Trends Cardiovasc Med, 2001. **11**(2): p. 49-54.
14. Benjamin, E.J., M.J. Blaha, S.E. Chiuve, M. Cushman, S.R. Das, R. Deo, . . . S. Stroke Statistics, *Heart Disease and Stroke Statistics-2017 Update: A Report From the American Heart Association.* Circulation, 2017. **135**(10): p. e146-e603.
15. Pekkan, K., L.P. Dasi, D. de Zelicourt, K.S. Sundareswaran, M.A. Fogel, K.R. Kanter, and A.P. Yoganathan, *Hemodynamic performance of stage-2 univentricular reconstruction: Glenn vs. hemi-Fontan templates.* Ann Biomed Eng, 2009. **37**(1): p. 50-63.
16. Liu, C., W. Liu, J. Palie, M.F. Lu, N.A. Brown, and J.F. Martin, *Pitx2c patterns anterior myocardium and aortic arch vessels and is required for local cell movement into atrioventricular cushions.* Development, 2002. **129**(21): p. 5081-91.
17. Wang, Y., O. Dur, M.J. Patrick, J.P. Tinney, K. Tobita, B.B. Keller, and K. Pekkan, *Aortic arch morphogenesis and flow modeling in the chick embryo.* Ann Biomed Eng, 2009. **37**(6): p. 1069-81.
18. Kowalski, W.J., O. Dur, Y. Wang, M.J. Patrick, J.P. Tinney, B.B. Keller, and K. Pekkan, *Critical transitions in early embryonic aortic arch patterning and hemodynamics.* PLoS One, 2013. **8**(3): p. e60271.

19. Goktas, S., F.E. Uslu, W.J. Kowalski, E. Ermek, B.B. Keller, and K. Pekkan, *Time-Series Interactions of Gene Expression, Vascular Growth and Hemodynamics during Early Embryonic Arterial Development.* PLoS One, 2016. **11**(8): p. e0161611.
20. Groenendijk, B.C., B.P. Hierck, A.C. Gittenberger-De Groot, and R.E. Poelmann, *Development-related changes in the expression of shear stress responsive genes KLF-2, ET-1, and NOS-3 in the developing cardiovascular system of chicken embryos.* Dev Dyn, 2004. **230**(1): p. 57-68.
21. Al Naieb, S., C.M. Happel, and T.M. Yelbuz, *A detailed atlas of chick heart development in vivo.* Ann Anat, 2013. **195**(4): p. 324-41.
22. Livak, K.J. and T.D. Schmittgen, *Analysis of relative gene expression data using real-time quantitative PCR and the 2(-Delta Delta C(T)) Method.* Methods, 2001. **25**(4): p. 402-8.
23. Vasilief, I., *QtiPlot - Data Analysis and Scientific Visualization*. 2017.
24. Szklarczyk, D., A. Franceschini, S. Wyder, K. Forslund, D. Heller, J. Huerta-Cepas, . . . C. von Mering, *STRING v10: protein-protein interaction networks, integrated over the tree of life.* Nucleic Acids Res, 2015. **43**(Database issue): p. D447-52.
25. Augustin, H.G., G.Y. Koh, G. Thurston, and K. Alitalo, *Control of vascular morphogenesis and homeostasis through the angiopoietin-Tie system.* Nat Rev Mol Cell Biol, 2009. **10**(3): p. 165-77.
26. Yancopoulos, G.D., S. Davis, N.W. Gale, J.S. Rudge, S.J. Wiegand, and J. Holash, *Vascular-specific growth factors and blood vessel formation.* Nature, 2000. **407**(6801): p. 242-8.
27. Chlench, S., N. Mecha Disassa, M. Hohberg, C. Hoffmann, T. Pohlkamp, G. Beyer, . . . A. Zakrzewicz, *Regulation of Foxo-1 and the angiopoietin-2/Tie2 system by shear stress.* FEBS Lett, 2007. **581**(4): p. 673-80.
28. Tressel, S.L., R.P. Huang, N. Tomsen, and H. Jo, *Laminar shear inhibits tubule formation and migration of endothelial cells by an angiopoietin-2 dependent mechanism.* Arterioscler Thromb Vasc Biol, 2007. **27**(10): p. 2150-6.
29. Goettsch, W., C. Gryczka, T. Korff, E. Ernst, C. Goettsch, J. Seebach, . . . H. Morawietz, *Flow-dependent regulation of angiopoietin-2.* J Cell Physiol, 2008. **214**(2): p. 491-503.
30. Li, R., T. Beebe, N. Jen, F. Yu, W. Takabe, M. Harrison, . . . T.K. Hsiai, *Shear stress-activated Wnt-angiopoietin-2 signaling recapitulates vascular repair in zebrafish embryos.* Arterioscler Thromb Vasc Biol, 2014. **34**(10): p. 2268-75.
31. Noria, S., D.B. Cowan, A.I. Gotlieb, and B.L. Langille, *Transient and steady-state effects of shear stress on endothelial cell adherens junctions.* Circ Res, 1999. **85**(6): p. 504-14.
32. Yamamoto, K., T. Takahashi, T. Asahara, N. Ohura, T. Sokabe, A. Kamiya, and J. Ando, *Proliferation, differentiation, and tube formation by endothelial progenitor cells in response to shear stress.* J Appl Physiol (1985), 2003. **95**(5): p. 2081-8.
33. Egorova, A.D., K. Van der Heiden, S. Van de Pas, P. Vennemann, C. Poelma, M.C. DeRuiter, . . . B.P. Hierck, *Tgfbeta/Alk5 signaling is required for shear stress induced klf2 expression in embryonic endothelial cells.* Dev Dyn, 2011. **240**(7): p. 1670-80.
34. Dekker, R.J., S. van Soest, R.D. Fontijn, S. Salamanca, P.G. de Groot, E. VanBavel, . . . A.J. Horrevoets, *Prolonged fluid shear stress induces a distinct set of endothelial cell genes, most specifically lung Kruppel-like factor (KLF2).* Blood, 2002. **100**(5): p. 1689-98.
35. Malek, A. and S. Izumo, *Physiological fluid shear stress causes downregulation of endothelin-1 mRNA in bovine aortic endothelium.* Am J Physiol, 1992. **263**(2 Pt 1): p. C389-96.
36. Mahler, G.J., C.M. Frendl, Q. Cao, and J.T. Butcher, *Effects of shear stress pattern and magnitude on mesenchymal transformation and invasion of aortic valve endothelial cells.* Biotechnol Bioeng, 2014. **111**(11): p. 2326-37.

37. Girard, P.R. and R.M. Nerem, *Shear stress modulates endothelial cell morphology and F-actin organization through the regulation of focal adhesion-associated proteins.* J Cell Physiol, 1995. **163**(1): p. 179-93.
38. Hartsock, A. and W.J. Nelson, *Adherens and tight junctions: structure, function and connections to the actin cytoskeleton.* Biochim Biophys Acta, 2008. **1778**(3): p. 660-9.
39. Resnick, N., H. Yahav, A. Shay-Salit, M. Shushy, S. Schubert, L.C. Zilberman, and E. Wofovitz, *Fluid shear stress and the vascular endothelium: for better and for worse.* Prog Biophys Mol Biol, 2003. **81**(3): p. 177-99.
40. Vestweber, D., *VE-cadherin: the major endothelial adhesion molecule controlling cellular junctions and blood vessel formation.* Arterioscler Thromb Vasc Biol, 2008. **28**(2): p. 223-32.
41. Tzima, E., M. Irani-Tehrani, W.B. Kiosses, E. Dejana, D.A. Schultz, B. Engelhardt, . . . M.A. Schwartz, *A mechanosensory complex that mediates the endothelial cell response to fluid shear stress.* Nature, 2005. **437**(7057): p. 426-31.
42. Doetschman, T., J.V. Barnett, R.B. Runyan, T.D. Camenisch, R.L. Heimark, H.L. Granzier, . . . M. Azhar, *Transforming growth factor beta signaling in adult cardiovascular diseases and repair.* Cell Tissue Res, 2012. **347**(1): p. 203-23.
43. Goumans, M.J., Z. Liu, and P. ten Dijke, *TGF-beta signaling in vascular biology and dysfunction.* Cell Res, 2009. **19**(1): p. 116-27.
44. Molin, D.G., R.E. Poelmann, M.C. DeRuiter, M. Azhar, T. Doetschman, and A.C. Gittenberger-de Groot, *Transforming growth factor beta-SMAD2 signaling regulates aortic arch innervation and development.* Circ Res, 2004. **95**(11): p. 1109-17.
45. Azhar, M., J. Schultz Jel, I. Grupp, G.W. Dorn, 2nd, P. Meneton, D.G. Molin, . . . T. Doetschman, *Transforming growth factor beta in cardiovascular development and function.* Cytokine Growth Factor Rev, 2003. **14**(5): p. 391-407.
46. Rundhaug, J.E., *Matrix metalloproteinases and angiogenesis.* J Cell Mol Med, 2005. **9**(2): p. 267-85.
47. Milkiewicz, M., C. Uchida, E. Gee, T. Fudalewski, and T.L. Haas, *Shear stress-induced Ets-1 modulates protease inhibitor expression in microvascular endothelial cells.* J Cell Physiol, 2008. **217**(2): p. 502-10.
48. Belo, V.A., D.A. Guimaraes, and M.M. Castro, *Matrix Metalloproteinase 2 as a Potential Mediator of Vascular Smooth Muscle Cell Migration and Chronic Vascular Remodeling in Hypertension.* J Vasc Res, 2015. **52**(4): p. 221-31.
49. Forstermann, U. and W.C. Sessa, *Nitric oxide synthases: regulation and function.* Eur Heart J, 2012. **33**(7): p. 829-37, 837a-837d.
50. Rimkus, T.K., R.L. Carpenter, S. Qasem, M. Chan, and H.W. Lo, *Targeting the Sonic Hedgehog Signaling Pathway: Review of Smoothened and GLI Inhibitors.* Cancers (Basel), 2016. **8**(2).
51. Washington Smoak, I., N.A. Byrd, R. Abu-Issa, M.M. Goddeeris, R. Anderson, J. Morris, . . . E.N. Meyers, *Sonic hedgehog is required for cardiac outflow tract and neural crest cell development.* Dev Biol, 2005. **283**(2): p. 357-72.
52. Vitelli, F., M. Morishima, I. Taddei, E.A. Lindsay, and A. Baldini, *Tbx1 mutation causes multiple cardiovascular defects and disrupts neural crest and cranial nerve migratory pathways.* Hum Mol Genet, 2002. **11**(8): p. 915-22.
53. Lindsay, E.A., F. Vitelli, H. Su, M. Morishima, T. Huynh, T. Pramparo, . . . A. Baldini, *Tbx1 haploinsufficieny in the DiGeorge syndrome region causes aortic arch defects in mice.* Nature, 2001. **410**(6824): p. 97-101.
54. Jerome, L.A. and V.E. Papaioannou, *DiGeorge syndrome phenotype in mice mutant for the T-box gene, Tbx1.* Nat Genet, 2001. **27**(3): p. 286-91.

55. Garg, V., C. Yamagishi, T. Hu, I.S. Kathiriya, H. Yamagishi, and D. Srivastava, *Tbx1, a DiGeorge syndrome candidate gene, is regulated by sonic hedgehog during pharyngeal arch development.* Dev Biol, 2001. **235**(1): p. 62-73.
56. Abu-Issa, R., G. Smyth, I. Smoak, K. Yamamura, and E.N. Meyers, *Fgf8 is required for pharyngeal arch and cardiovascular development in the mouse.* Development, 2002. **129**(19): p. 4613-25.
57. Frank, D.U., L.K. Fotheringham, J.A. Brewer, L.J. Muglia, M. Tristani-Firouzi, M.R. Capecchi, and A.M. Moon, *An Fgf8 mouse mutant phenocopies human 22q11 deletion syndrome.* Development, 2002. **129**(19): p. 4591-603.
58. Vitelli, F., I. Taddei, M. Morishima, E.N. Meyers, E.A. Lindsay, and A. Baldini, *A genetic link between Tbx1 and fibroblast growth factor signaling.* Development, 2002. **129**(19): p. 4605-11.
59. Jackson, A., S. Kasah, S.L. Mansour, B. Morrow, and M.A. Basson, *Endoderm-specific deletion of Tbx1 reveals an FGF-independent role for Tbx1 in pharyngeal apparatus morphogenesis.* Dev Dyn, 2014. **243**(9): p. 1143-51.
60. Zhang, Z., F. Cerrato, H. Xu, F. Vitelli, M. Morishima, J. Vincentz, . . . E. Lindsay, *Tbx1 expression in pharyngeal epithelia is necessary for pharyngeal arch artery development.* Development, 2005. **132**(23): p. 5307-15.
61. Yanagisawa, H., R.E. Hammer, J.A. Richardson, S.C. Williams, D.E. Clouthier, and M. Yanagisawa, *Role of Endothelin-1/Endothelin-A receptor-mediated signaling pathway in the aortic arch patterning in mice.* J Clin Invest, 1998. **102**(1): p. 22-33.
62. Kurihara, Y., H. Kurihara, H. Oda, K. Maemura, R. Nagai, T. Ishikawa, and Y. Yazaki, *Aortic arch malformations and ventricular septal defect in mice deficient in endothelin-1.* J Clin Invest, 1995. **96**(1): p. 293-300.
63. Morishima, M., H. Yanagisawa, M. Yanagisawa, and A. Baldini, *Ece1 and Tbx1 define distinct pathways to aortic arch morphogenesis.* Dev Dyn, 2003. **228**(1): p. 95-104.
64. Trumpp, A., M.J. Depew, J.L. Rubenstein, J.M. Bishop, and G.R. Martin, *Cre-mediated gene inactivation demonstrates that FGF8 is required for cell survival and patterning of the first branchial arch.* Genes Dev, 1999. **13**(23): p. 3136-48.
65. Srivastava, D., *HAND proteins: molecular mediators of cardiac development and congenital heart disease.* Trends Cardiovasc Med, 1999. **9**(1-2): p. 11-8.
66. Thomas, T., H. Kurihara, H. Yamagishi, Y. Kurihara, Y. Yazaki, E.N. Olson, and D. Srivastava, *A signaling cascade involving endothelin-1, dHAND and msx1 regulates development of neural-crest-derived branchial arch mesenchyme.* Development, 1998. **125**(16): p. 3005-14.
67. Srivastava, D., T. Thomas, Q. Lin, M.L. Kirby, D. Brown, and E.N. Olson, *Regulation of cardiac mesodermal and neural crest development by the bHLH transcription factor, dHAND.* Nat Genet, 1997. **16**(2): p. 154-60.
68. Kameda, Y., *Hoxa3 and signaling molecules involved in aortic arch patterning and remodeling.* Cell Tissue Res, 2009. **336**(2): p. 165-78.
69. Kameda, Y., T. Nishimaki, M. Takeichi, and O. Chisaka, *Homeobox gene hoxa3 is essential for the formation of the carotid body in the mouse embryos.* Dev Biol, 2002. **247**(1): p. 197-209.
70. Gorski, D.H. and K. Walsh, *Control of vascular cell differentiation by homeobox transcription factors.* Trends Cardiovasc Med, 2003. **13**(6): p. 213-20.
71. Cantile, M., G. Schiavo, L. Terracciano, and C. Cillo, *Homeobox genes in normal and abnormal vasculogenesis.* Nutr Metab Cardiovasc Dis, 2008. **18**(10): p. 651-8.
72. Nakagawa, T., M. Abe, T. Yamazaki, H. Miyashita, H. Niwa, S. Kokubun, and Y. Sato, *HEX acts as a negative regulator of angiogenesis by modulating the expression of*

angiogenesis-related gene in endothelial cells in vitro. Arterioscler Thromb Vasc Biol, 2003. **23**(2): p. 231-7.
73. Duband, J.L. and J.P. Thiery, *Distribution of laminin and collagens during avian neural crest development.* Development, 1987. **101**(3): p. 461-78.
74. Chiang, H.Y., V.A. Korshunov, A. Serour, F. Shi, and J. Sottile, *Fibronectin is an important regulator of flow-induced vascular remodeling.* Arterioscler Thromb Vasc Biol, 2009. **29**(7): p. 1074-9.
75. Sottile, J., F. Shi, I. Rublyevska, H.Y. Chiang, J. Lust, and J. Chandler, *Fibronectin-dependent collagen I deposition modulates the cell response to fibronectin.* Am J Physiol Cell Physiol, 2007. **293**(6): p. C1934-46.
76. Goktas, S., C. Karakaya, A.I. Cakiroglu, M. Celik, S. Karahuseyinoglu, and K. Pekkan, *Microstructural remodeling patterns in early aortic arch development.*
77. Johnson, D.J., P. Robson, Y. Hew, and F.W. Keeley, *Decreased elastin synthesis in normal development and in long-term aortic organ and cell cultures is related to rapid and selective destabilization of mRNA for elastin.* Circ Res, 1995. **77**(6): p. 1107-13.
78. Eichner, R. and J. Rosenbloom, *Collagen and elastin synthesis in the developing chick aorta.* Arch Biochem Biophys, 1979. **198**(2): p. 414-23.
79. Tokimitsu, I., S. Tajima, T. Nishikawa, M. Tajima, and T. Fukasawa, *Sequence analysis of elastin cDNA from chick aorta and tissue-specific transcription of the elastin gene in developing chick embryo.* Arch Biochem Biophys, 1987. **256**(2): p. 455-61.
80. Wagenseil, J.E. and R.P. Mecham, *Vascular extracellular matrix and arterial mechanics.* Physiol Rev, 2009. **89**(3): p. 957-89.
81. Colas, J.F., A. Lawson, and G.C. Schoenwolf, *Evidence that translation of smooth muscle alpha-actin mRNA is delayed in the chick promyocardium until fusion of the bilateral heart-forming regions.* Dev Dyn, 2000. **218**(2): p. 316-30.
82. Carisey, A. and C. Ballestrem, *Vinculin, an adapter protein in control of cell adhesion signalling.* Eur J Cell Biol, 2011. **90**(2-3): p. 157-63.
83. Huveneers, S., J. Oldenburg, E. Spanjaard, G. van der Krogt, I. Grigoriev, A. Akhmanova, . . . J. de Rooij, *Vinculin associates with endothelial VE-cadherin junctions to control force-dependent remodeling.* J Cell Biol, 2012. **196**(5): p. 641-52.
84. Mallat, Z. and A. Tedgui, *Apoptosis in the vasculature: mechanisms and functional importance.* Br J Pharmacol, 2000. **130**(5): p. 947-62.
85. McIlwain, D.R., T. Berger, and T.W. Mak, *Caspase functions in cell death and disease.* Cold Spring Harb Perspect Biol, 2013. **5**(4): p. a008656.
86. Franceschini, A., D. Szklarczyk, S. Frankild, M. Kuhn, M. Simonovic, A. Roth, . . . L.J. Jensen, *STRING v9.1: protein-protein interaction networks, with increased coverage and integration.* Nucleic Acids Res, 2013. **41**(Database issue): p. D808-15.
87. von Mering, C., L.J. Jensen, B. Snel, S.D. Hooper, M. Krupp, M. Foglierini, . . . P. Bork, *STRING: known and predicted protein-protein associations, integrated and transferred across organisms.* Nucleic Acids Res, 2005. **33**(Database issue): p. D433-7.

Appendix A. Experimental Protocols

Protocol A1: Total RNA Extraction/Purification Protocol

Materials:

- GeneJET RNA purification kit (Thermo Scientific-K0732)
- Absolute Ethanol (EtOH)
- 14.3 M β-mercaptoethanol (Sigma Aldrich, M6250)
- TE buffer (10 mM Tris HCl, pH 8.0, 1 mM EDTA) (Thermo Scientific-17890)
- Vortex
- Microcentrifuge

Procedure:

1) In cell culture lab, put 1180 µL of TE buffer into 4 centrifuge tubes.

2) In cell culture lab, put 1500 µL lysis buffer in 2 centrifuge tubes.

3) Under the fume hood, add 30 µL of 14.3 M β-mercaptoethanol onto the 1500 µL Lysis Buffer.

4) Put 300 µL of Lysis Buffer supplemented with β-mercaptoethanol to each 1.5 ml centrifuge tubes (number depends on the sample types).

5) Put all the samples in the lysis buffer, and vortex for 10 s to mix thoroughly.

6) Take the samples to the cell culture lab.

7) Under the hood, put 20 µL of Proteinase K to each tube containing TE buffer.

8) Add 600 µL of diluted Proteinase K solution to each tube containing the samples.

9) Vortex and incubate at 15-25ºC for 10 min.

10) Centrifuge for 5 min at 12000 xg. Transfer the supernatant (about 870 µl) into a new centrifuge tube.

11) Add 450 µL of absolute EtOH and mix by pipetting.

12) Transfer 500 µL of mixture to the GeneJET RNA Purification Column inserted in a collection tube.

13) Centrifuge the column for 1 min at 12000 xg. Discard the flow-through and place the purification column back into the collection tube.

- Repeat step 12 & 13 until all mixture is transferred to the column and centrifuged.

14) Discard the collection tube containing the flow-through solution.

15) Place the purification column into a new 2 ml collection tube.

16) Add Wash Buffer 1 (700 µL) to the purification column.

17) Centrifuge the column with collection tube for 1 min at 12000 xg.

18) Discard the flow-through and place the purification column back into the collection tube.

19) Add Wash Buffer 2 (600 µL) to the purification column.

20) Centrifuge the column with collection tube for 1 min at 12000 xg.

21) Discard the flow-through and place the purification column back into the collection tube.

22) Add Wash Buffer 2 (250 µL) to the purification column.

23) Centrifuge the column with collection tube for 2 min at 12000 xg.

24) Discard the collection tube containing the flow-through solution and transfer the purification column to a sterile 1.5 mL Eppendorf tube.

25) Add distilled water (50 µL) to the center of the purification column membrane. Centrifuge it for 1 min at 12000 xg to obtain RNA.

26) Repeat step 25 one more time.

27) Discard the purification column and keep the Eppendorf tube containing purified RNA for downstream applications or store RNA at -80ºC until use.

28) Take 9 µL of purified RNA for nanodrop measurement.

Protocol A2: cDNA Synthesis from Extracted RNA

Materials:

- Rapidout DNA Removal Kit – put on ice during the experiment
  - 10X DNase buffer with $MgCl_2$
  - DNase I, RNase-free
  - DNase Removal Reagent (DRR)
- Maxima First Strand cDNA Synthesis Kit – put on ice during the experiment
  - 5X Reaction Mix
  - Maxima Enzyme Mix
  - Water, nuclease-free

Procedure:

Removal of Genomic DNA from Total RNA Preparations

1) According to the RNA concentration measurements obtained with NanoDrop, make the concentrations of the RNA samples equal by adding the required amounts of nuclease-free water.

2) Mix the components in Table A.1 in Eppendorf tubes. Mix them with pipetting.

Table A.1: Ingredients and required amounts for genomic DNA removal

Component	**Amount**
RNA sample	85 µL
10X DNase buffer with $MgCl_2$	10 µL
DNase I, RNase-free	5 µL
Total	**100 µL**

3) Incubate the mixture at 37ºC for 30 min.

DNase Removal

1) Prior each use, vortex DRR until completely resuspended.

2) Add 10 µL of DRR to the mixture.

3) Incubate at room temperature by gently mixing 2-3 times to resuspend the DRR.

4) Centrifuge the tube at 1200xg for 1 min.

5) Transfer the supernatant, containing RNA into a new tube (almost 93 µL). Do not take pellet including DRR.

First Strand cDNA Synthesis

1) Add the solutions as indicated order in Table A.2 into an Eppendorf tube on ice.

Table A.2: Ingredients and required amounts to prepare mastermix for cDNA synthesis

	1 tube	Mastermix for 25 tubes
5X Reaction Mix	8µL	200 µL
Maxima Enzyme Mix	4 µL	100 µL
Template RNA	22 µL	-
Water, nuclease-free	6 µL	150 µL
Total volume	40 L	

2) Divide the mastermix as 18 µL to each empty Eppendorf tube, then add 22 µL of the template RNA. Mix gently by pipetting.

3) Incubate the mixture at 25˚C for 10 min

4) Incubate the mixture at 50˚C for 15 min.

5) Incubate the mixture at 85˚C for 5 min to stop the reaction.

6) Store the synthesized cDNA at 20˚C for up to one week, or at -80˚C is for longer period.

Protocol A3: RT-qPCR Protocol

Materials:

- Luminaris Color HiGreen qPCR Master Mix
- Reverse and Forward Primers
- Distilled Water

Procedure:

1) According to the number of genes that will be analyzed, multiply the amounts for each well with well number to determine the total amounts in mastermix as in Table A.3.

Table A.3: Ingredients and required amounts of solutions for RT-qPCR mastermix preparation

Solution	**Well Number**	**Amount for each well**	**Total amount in mastermix**
Luminaris Color HiGreen qPCR Master Mix	20	10 µL	200 µL
Reverse Primer	20	0.6 µL	12 µL
Forward Primer	20	0.6 µL	12 µL
Water	20	6.8 µL	136 µL

*Well number can change according to the experiment. If so, recalculate the total amount in mastermix.

2) Divide the mastermix into the wells. Each well should include 18 µL of mastermix.

3) Add 2 µL of corresponding cDNA into the wells.

4) Seal the plate properly.

5) Place the plate into the RT-qPCR cycler, and start the run with using the software.

Protocol A4: STRING Database Usage

Proteins are the functional products of genes. To understand the relations between protein-encoding genes, protein-protein interactions can be beneficial. There are several databases to provide the interactions, but STRING (Search Tool for the Retrieval of Interacting Genes/Proteins) is one of the most user-friendly and comprehensive databases. [86]

STRING is an online resource (http://string-db.org) which provides protein-protein interactions of more than 2000 organisms. The interactions include both direct (physical) and indirect (functional) associations, and derived from the computational analysis of known and predicted interactions. It uses multiple sources to determine the interactions; primary databases are used to import known experimental interactions, manually curated databases are used to get the pathway knowledge, Medline abstracts and full-text articles are used, some algorithms utilizing co-expression and genomic information are used to predict the *de novo* interactions, and orthology relations are used to determine the interactions in one organism and transfer it to the other [24].

STRING computes combined scores to determine the protein-protein interactions. It basically combines the probabilities from different evidences. Moreover, some corrections are done for randomly observed interactions [87].

As a starting point, the list of desired genes/proteins were entered to the STRING search box with the selection of 'Multiple Proteins'. STRING can understand the names of proteins, but for accuracy, the IDs of proteins obtained from Ensemble and RefSeq were used since STRING imports its sequences from those resources. The organism was specified as *Gallus Gallus*, and the search was started. In the opening window, the names and the functions of the proteins were double-checked. It was seen that STRING could not find some genes/proteins such as TBX1 and NOS3, so the same procedure was repeated for the organism *Homo Sapiens*, and STRING found all of the genes/proteins in the list. After this step, the protein network appeared.

The protein network view summarizes the predicted associations between selected proteins. The nodes represent the proteins while the edges represent the predicted functional associations. In the settings, the meaning of network edges can be adjusted based on evidence, confidence or molecular action. If the evidence mode is selected, different line colors will represent the different kinds of interaction evidences. If the confidence mode is selected, the line thickness will indicate the strength of the data. If the action mode is selected, the lines will represent the predicted mode of actions such as binding, activation and inhibition. The network display mode provides the users to change the format of the network. The interactive flash network enables to cluster the proteins. The analysis part gives some statistics about the network. It also shows the functional enrichments for gene ontologies and pathways.

The parameters determining the network can be changed with navigation buttons. In the data settings, the active interaction sources can be changed with including or excluding text-mining, experimental, database and co-expression, neighborhood, gene fusion and co-occurrence, evidences. Text-mining results show significant protein-protein interactions extracted from the abstracts of the scientific papers. Experiment results show significant protein-protein interactions obtained from other databases. They are acquired from BIND, DIP, GRID, HPRD, IntAct, MINT and PID. Database results show significant protein-protein interactions obtained from curated databases. They are acquired from Biocarta, BioCyc, GO, KEGG and Reactome. Co-expression results show the genes that are expressed together in the same or in other species. Neighborhood results show the genes that are in close to each other in the genome. Gene fusion results show the gene fusion event, which is the formation of a hybrid gene from two separate genes, per species. Co-occurrence results show the presence or absence of proteins across species within their phylogeny. Furthermore, the minimum required interaction score can be adjusted to put a threshold to the confidence scores. It is adjusted to 0.4 (medium confidence), and the highest confidence score is 0.9, but still any desired custom value can be given to the system.

After the appearance of the network, default parameters were used. All of the active interaction sources were selected, and minimum required interaction score was adjusted to 0.400. In the basic settings, molecular action was selected for the meaning of edges, and interactive network was selected for the display mode. Nodes of the network was aligned as desired, and exported as high-resolution image.

Appendix B. Additional Studies on Chick Embryonic Cardiomyocytes

Our first aim was to determine an optimal protocol for primary cardiomyocyte culture from embryonic chick hearts to be used in further experiments. For that purpose, several protocols were tried. In general, protocols included, first the removal of the heart from the embryo, following with a digestion process, and finally cell harvesting and culturing step. Major differences between the protocols were in the trypsinization process (different amounts of enzymes, different time intervals) and the ingredients of the mediums used.

It is known that L-glutamine in the medium promotes fibroblast growth. High fetal bovine serum (FBS) concentration also promotes fibroblast growth since they cannot proliferate in low FBS environment. Furthermore, pre-plating is a crucial step because fibroblasts can attach the surface in 1-2 hours while cardiomyocytes can attach in 10-12 hours, so this step provides us to eliminate many fibroblasts before the actual incubation. The optimal protocol was prepared accordingly (Protocol B1), and used to isolate synchronously beating cardiomyocyte population. Moreover, immunofluorescence (IF) staining (Protocol B2 and B3) were used to visualize cardiomyocytes and determine the pureness of the plates in terms of the isolation and growth of non-cardiomyocyte cells.

Protocol B1: Cardiomyocyte Isolation from Chick Embryos

Mediums:

Trypsin solution: 0.1% trypsin in Ca- and Mg-free HBSS

Nutrient medium: 10% FBS, 1%penstrep in MEM with glutamine

Growth medium: 5% FBS, 1%penstrep in MEM without glutamine

Procedure:

1) Incubate the fertile eggs at 37.5°C incubator with 67% relative humidity until day 5.

2) Sterilize the surface of the egg with 70% EtOH, and perform the dissociation into the hood.

3) Tap the egg with the end of a sterile forceps about one-fourth of the way down from the blunt end.

4) Use the forceps to break away small fragments of shell around the circumference until the cap can be removed.

5) With fine forceps and a sterile metal spoon, lift the embryo by its neck into a sterile Petri dish (100-mm).

6) Remove its head from the body, and separate the heart from the embryo with fine forceps and scissors.

7) Place the separated heart into a sterile Petri dish containing HBSS (Ca and Mg-free) on ice.

8) Remove the excess connective tissue and place the heart into a second petri dish of HBSS (Ca and Mg-free) on ice.

9) Chop the heart into small (e.g. 1 mm) pieces.

10) Pipette off the HBSS and reintroduce the HBSS into the Petri dish.

   a. Make sure that there is not a tissue in the tip of the pipette.

b. Make sure that the tissues are not dry.

11) Repeat 'step 10' until HBSS looks clean. Leave some HBSS after final rinse.

12) Transfer the tissues into a falcon tube (15 ml).

a. Make sure that there is some HBSS left in the falcon tube.

---

13) Trypsinization preparation:

a. Add 10 ml prewarmed trypsin solution into the tube, and incubate them for 10 min at 37 C in 5% CO2 incubator.

b. Discard supernatant from Trypsinization preparation.

14) Trypsinization:

a. Add 3.5 ml fresh prewarmed trypsin solution, and incubate for 8 min.

b. Collect supernatant, and place into 25 ml volume of nutrient medium.

15) Repeat 'Trypsinization' for several times (Tryp. 1, 2, 3 and 4).

---

16) Centrifuge the mixture containing nutrient medium and cells at 1000 rpm for 10 min.

17) Discard the supernatant by tilting the tube (if not sure, use pipettes), and take out the remaining solution with micropipette.

18) Resuspend the pellet (cells) with 4 ml of nutrient medium. (pipette up and down)

19) Preplate the suspension on a sterile 60-mm Petri dish, and maintain in a 5% CO2 incubator at 37C for 1 hour.

---

20) After the attachment of fibroblasts, collect the suspended cells into a falcon tube (15 ml).

21) In an Eppendorf tube, add 10 μL of trypan blue and 10 μL of cell suspension.

22) Inject 10 μL of the mixture on the sides of the hemocytometer for cell counting.

23) Count the cells in the hemocytometer under the microscope (viable and dead cells).

---

24) Culture the cells in 12-well plate including coverslips and 24-well plate in 5% CO2 at 37C.

25) One day after plating, replace the nutrient medium with growth medium.

26) Replace the growth medium every second day.

References:

1) Salameh A. and Dhein S. *Culture of Neonatal Cardiomyocytes,* Cell Culture Techniques, Ch5.2, p. 568-576.

2) Lin, Z.X., et al., *Polygons and adhesion plaques and the disassembly and assembly of myofibrils in cardiac myocytes.* J Cell Biol, 1989. **108**(6): p. 2355-67.

3) Wu, J.C., et al., *N-cadherin/catenin-based costameres in cultured chicken cardiomyocytes.* J Cell Biochem, 1999. **75**(1): p. 93-104.

Protocol B2: Click-iT EdU Staining Protocol

Materials

- Click-iT Plus EdU Imaging Kits (Invitrogen-C10637)
- 3.7% formaldehyde in PBS
- Wash Solution = 3% bovine serum albumin (BSA) in PBS
- Permeabilization Buffer = PBS containing 0.5% Triton X-100
- Distilled water

Preparation

1) Component A (10 mM stock solution): Add 2 ml DMSO (Component C) to EdU. Store the stock solution at -20C for up to 1 year.

2) Component A (2X working solution): Mix stock solution of Component A with complete cell medium to have a concentration of 10µM EdU.

3) Component B working solution: Add 70 µl DMSO (Component C) to AlexaFluor azide. Store the stock solution at -20C for up to 1 year.

4) Component D working solution (1X): Add 4 ml of Click-iT EdU reaction buffer (all solution in the bottle) into 36 ml distilled water. Store at 4C for up to 6 months.

5) Component F (10X stock solution): Add 2 ml of distilled water into Click-iT EdU buffer additive. Store at -20C for up to 1 year.

6) Component F (1X working solution): Dilute Component F 10X stock solution with distilled water (1:10). **Important:** use the working solution on the same day.

Procedure

1) Prepare the stock solutions, and then the working solutions.

2) Grow the cells onto glass coverslips within the plates.

3) Discard half of the cell media in well plates, and add 2X Component A (EdU working solution), thus, final EdU solution will be 1X.

4) Incubate the cells overnight.

5) The other day, remove the media, add each well 3.7% formaldehyde in PBS, and incubate for 15 min at room temperature.

6) Discard the solution, and wash the cells with wash solution twice.

7) Discard the solution, add permeabilization buffer, and incubate for 20 min at room temperature.

8) Freshly prepare Click-iT reaction cocktail by adding the solution with the same order as in Table B.1. **Important:** Use the cocktail within 15 min.

Table B.1: Click-iT reaction cocktail ingredients

Ingredients	**Volume for 1 coverslip**
1X Click-iT Reaction Buffer (Component D)	430 µl
$CuSO_4$ (Component E)	20 µl
Component B working solution (Alexa Fluor azide)	1.2 µl
Reaction buffer additive (Component F)	50 µl
Total Volume	**500 µl**

9) After removing the permeabilization buffer, wash the cells with wash solution twice.

10) Discard the wash solution.

11) Add reaction cocktail to wells (500 µl for each coverslip), and incubate for 30 min at room temperature in dark.

12) Discard the cocktail and wash the cells with wash solution once.

13) Discard the wash solution.

14) Proceed with Protocol B3 for immunofluorescence staining.

Protocol B3: Immunofluorescence Protocol for Sarcomeric a-actinin Staining of Cardiomyocytes

Materials:

- Wash buffer = 0.1% Tween 20 + 1x phosphate buffered saline (PBS).
- PFA solution = 4% Paraformaldehyde (PFA) in PBS (pH:7.4)
- PBS containing 0.2% Triton X-100
- Protein Block (Abcam-ab64226)
- Sarcomeric a-actinin antibody solution (Abcam- ab9465)
    - 1:100 diluted with PBS azide
- Goat Anti-mouse IgG H&L Alexa Fluor 488 (Abcam- ab150113)
    - 1:200 diluted with PBS azide
- Fluoroshield Mounting Medium with DAPI (Abcam-ab104139)

Procedure:

1) Grow the cells onto glass coverslip within well-plates.

2) Aspirate the medium and wash the cells briefly with wash buffer.

3) Fix the cells by adding PFA solution into the wells, and leave them 10 min at room temperature.

4) Wash the cells three times with ice-cold wash buffer.

5) Permeabilize the cells by incubating them with PBS containing 0.2% Triton X-100 for 10 min.

6) Wash the cells three times with ice-cold wash buffer.

7) Add 6-7 drops of Protein Block, and incubate the cells for 30 min.

8) Wash the cells once with ice-cold wash buffer.

9) Incubate the cells with 1:100 diluted sarcomeric a-actinin antibody solution for 1 hour at room temperature in the dark.

10) Discard the solution and wash the cells three times with wash buffer.

11) Incubate the cells with 1:200 diluted secondary antibody (goat-anti-mouse) solution for 1 hour at room temperature in the dark.

12) Discard the solution and wash the cells three times with wash buffer for 5 min each in the dark.

13) Mount the coverslip with mounting medium.

14) Seal the coverslip with nail polish.

15) Store in dark at -20C.

Results of Cardiomyocyte Experiments

Our first aim was to develop and optimize a cardiomyocyte isolation protocol from chick embryos, and maintain the culture for further experiments. The protocol and culturing should have allowed to the spontaneous and synchronous beating of cardiomyocytes within the culture plates as well as other cells types within the heart such as fibroblasts and EC should have found in lower quantities. Our results showed that isolated cardiomyocytes can beat spontaneously and spread through the plate (Figure B.1). Moreover, immunofluorescence staining of sarcomeric a-actinin, specific to cardiomyocytes, revealed the successful isolation of cardiomyocytes (Figure B.2). Click-iT EDU staining showed the proliferative behavior of embryonic cardiomyocytes (Figure B.3). Overall, the isolation and staining protocols for cardiomyocytes are ready to be used in future experimental purposes.

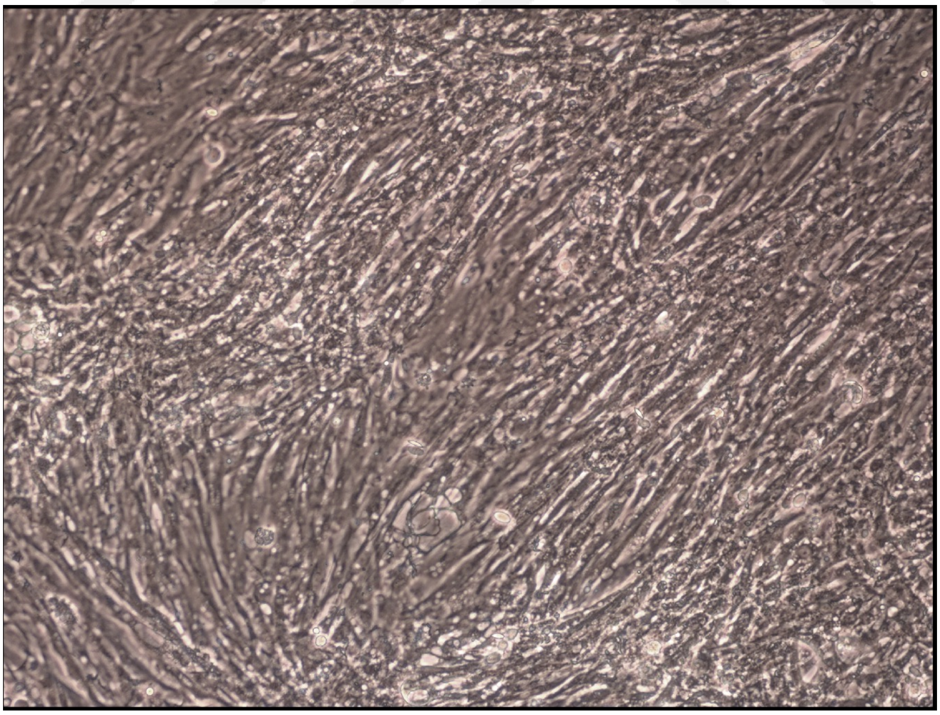

Figure B.1: Image of isolated and beating cardiomyocytes of 5-day old chick embryos in culture plate. The image was taken under microscope with 20X lens magnification.

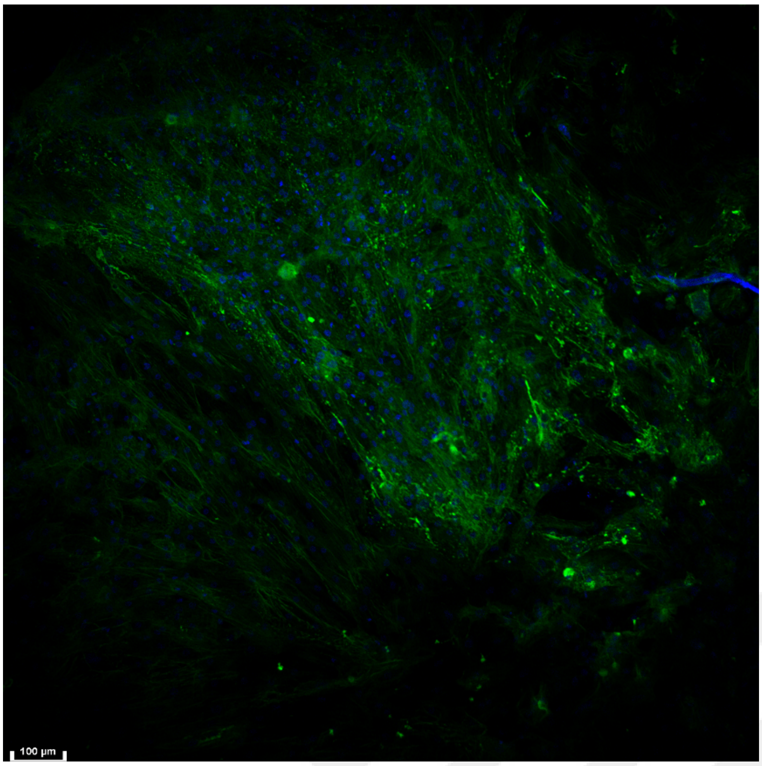

Figure B.2: Immunofluorescence staining of sarcomeric a-actinin (labelled with green) of isolated cardiomyocytes. DAPI stain is used to label cell nuclei. Image was taken under confocal microscope with 5x magnification.

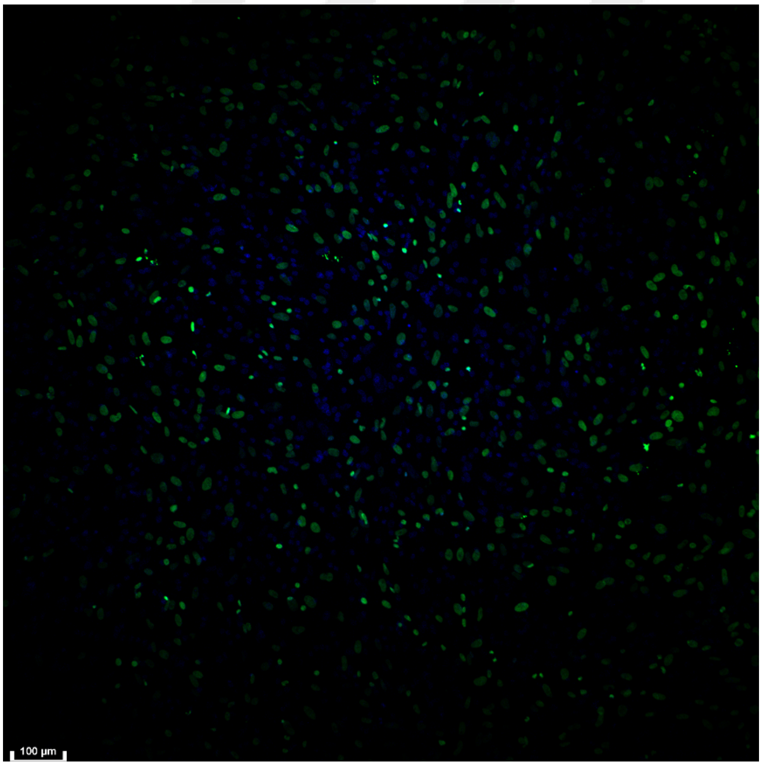

Figure B.3: Immunofluorescence staining of Click-iT EDU (green) of isolated cardiomyocytes. DAPI stain is used to label cell nuclei. Double stained cell nuclei denote proliferating cardiomyocytes. Image was taken under confocal microscope with 5x magnification.

Appendix C. Publications and Conference Proceedings

Publications:

1) Karakaya C., Goktas S., Celik M., Kowalski W.J., Keller B.B., Pekkan K. *Symmetry in Mechanosensitive Gene Expression during Aortic Arch Morphogenesis*, submitted.

2) Goktas S., Karakaya C., Cakiroglu A.I., Celik M., Karahuseyinoglu S., Pekkan K. *Microstructural remodeling patterns in early aortic arch development*, to be submitted.

Conferences:

1) Goktas S., Karakaya C., Karahuseyinoglu S., Pekkan K. *Flow-induced mechanics and gene expression patterns in microvascular great artery morphogenesis*. BMES Meeting, Tampa FL, October 7-10, 2015.

2) Karakaya C., Goktas S., Celik M., Pekkan K. *Cross-talk between morphogenetic proteins during development of embryonic great vessels*. EMBO Symposium: Mechanical Forces in Biology, Heidelberg, July 12-15, 2017.

3) Karakaya C., Goktas S., Celik M., Pekkan K. *Mechanosensitive gene expression in the morphogenesis of embryonic great vessels*. MolBiyoKon2017, Istanbul, September 8-10, 2017.

The experimental protocols prepared and submitted to the laboratory achieve are listed below.

1) Total RNA Extraction/Purification Protocol

2) cDNA Synthesis from Extracted RNA

3) RT-qPCR Protocol

4) STRING Database Usage

5) Cardiomyocyte Isolation from Chick Embryos

6) Click-iT EdU Staining Protocol

7) Immunofluorescence Protocol for Sarcomeric a-actinin Staining of Cardiomyocytes

8) F-actin Staining Protocol

9) Cell Counting Protocol

10) Collagen Coating Protocol

11) Gelatin Coating Protocol

12) Zebrafish Embryo Medium with Methylene Blue Protocol

13) Zebrafish Larva Maintenance Protocol

14) Zebrafish Breeding and Imaging Protocol

15) Artemia Hatching and Collection

16) Smart2Pure Water Purification System Handling

17) Waste Disposal Protocol